UC Irvine

UC Irvine Electronic Theses and Dissertations

Title

Global Observations of Oceanic Alkyl Nitrates and Dimethyl Sulfide During the NASA Atmospheric Tomography Mission (ATom)

Permalink

https://escholarship.org/uc/item/3g54g95r

Author

Woods, Christopher

Publication Date

2020

Peer reviewed|Thesis/dissertation

eScholarship.org Powered by the California Digital Library
University of California

UNIVERSITY OF CALIFORNIA,
IRVINE

Global Observations of Oceanic Alkyl Nitrates and Dimethyl Sulfide During the NASA Atmospheric Tomography Mission (ATom)

DISSERTATION

submitted in partial satisfaction of the requirements
for the degree of

DOCTOR OF PHILOSOPHY

in Chemistry

by

Christopher Thomas Woods

Dissertation Committee:
Professor Donald R. Blake, Chair
Professor Sergey Nizkorodov
Professor Barbara Finlayson-Pitts

2020

© 2020 Christopher Thomas Woods

DEDICATION

I dedicate this thesis to the people closest to me. To my parents, for always supporting the best version of me. To my brother, for always being the person I to look up to. And to my wonderful partner Mackenzie for being a fountain of positivity and unconditional love.

To the future scientists that use these historical data in their study of the ever-changing Earth System,

May it be invaluable in their Quest

"The barrel is the safest part of the wave"
- Jerry Lopez

'Over the Mountains
Of the Moon,
Down the Valley of the Shadow,
Ride, boldly ride,'
The shade replied,—
'If you seek for Eldorado!'

- E.A. Po

TABLE OF CONTENTS

LIST OF FIGURES

LIST OF TABLES

ACKNOWLEDGMENTS

I would like to express my deepest appreciation for my research advisor, Dr. Don Blake. Don, you are an excellent scientist, but you have never forgotten the human aspect. The culture that you cultivate in your research group and the way you positively enable and support their livelihood and success is too be commended. I also believe that I have this environment and these people to thank for making it through the graduate school process. Thank you for taking me in, thank you for letting me pursue my career my way and thank you for flying with me. I will always be ready for another flight on the DC-8 or another sampling trip.

Thank you to Professors Barbara Finlayson-Pitts and Sergey Nizkorodov, members of both my orals and dissertation committees. They have both pushed me to be the best scientist I could be, even when I was distracted with field work. They are exemplars of the scholar who is both excellent and kind.

Thank you to all Rowland-Blake lab members, past and present. We truly are a family. I appreciate the tutelage and the camaraderie. Alex, thank you for your time and for accepting my sense of humor. I would like to especially thank Simone, Brent and Gloria, for they are the absolute lifeblood of this research group. No student, myself included, would get far without your painstaking hard work, diligence and excellence.

Thank you to Barbara Chisholm. It is rare to work with a person who juggles so much, who is so indefatigable, yet will drop everything in a heartbeat to help someone. Thank you for getting me out of binds with passports, reimbursements, missed flights and hotels. It was a joy to work with you.

Thank you to my cohort, together we survived the trials and tribulations. It was a pleasure to get to be a part of such a diverse group. I look forward to future shenanigans.

To my friends, you kept me sane with surfing and fishing. Thank you

To coffee and metal music, thank you for being the rock I built my Ph.D. upon.

VITA

Christopher Thomas Woods

2013	A.S. in Chemistry, Saddleback College
2015	B.S. in Chemistry, University of California, Santa Barbara
2015-18	Teaching Assistant, Department of Chemistry, University of California, Irvine
2016-20	Research Assistant, Donald Blake Lab, University of California, Irvine
2018-19	Head Teaching Assistant, Department of Chemistry, University of California, Irvine
2018-19	Teaching Intern (CCCIP), Santa Ana College, Santa Ana
2019	M.S. in Chemistry, University of California, Irvine
2020	Ph.D. in Chemistry, University of California, Irvine

FIELD OF STUDY

Biogenic and anthropogenic volatile organic compounds in the remote atmosphere.

PUBLICATIONS

Wofsy, S.C., S. Afshar, H.M. Allen, E.C. Apel, E.C. Asher, B. Barletta, J. Bent, H. Bian, B.C. Biggs, D.R. Blake, N. Blake, I. Bourgeois, C.A. Brock, W.H. Brune, J.W. Budney, T.P. Bui, A. Butler, P. Campuzano-Jost, C.S. Chang, M. Chin, R. Commane, G. Correa, J.D. Crounse, P. D. Cullis, B.C. Daube, D.A. Day, J.M. Dean-Day, J.E. Dibb, J.P. DiGangi, G.S. Diskin, M. Dollner, J.W. Elkins, F. Erdesz, A.M. Fiore, C.M. Flynn, K.D. Froyd, D.W. Gesler, S.R. Hall, T.F. Hanisco, R.A. Hannun, A.J. Hills, E.J. Hintsa, A. Hoffman, R.S. Hornbrook, L.G. Huey, S. Hughes, J.L. Jimenez, B.J. Johnson, J.M. Katich, R.F. Keeling, M.J. Kim, A. Kupc, L.R. Lait, J.-F. Lamarque, J. Liu, K. McKain, R.J. Mclaughlin, S. Meinardi, D.O. Miller, S.A. Montzka, F.L. Moore, E.J. Morgan, D.M. Murphy, L.T. Murray, B.A. Nault, J.A. Neuman, P.A. Newman, J.M. Nicely, X. Pan, W. Paplawsky, J. Peischl, M.J. Prather, D.J. Price, E. Ray, J.M. Reeves, M. Richardson, A.W. Rollins, K.H. Rosenlof, T.B. Ryerson, E. Scheuer, G.P. Schill, J.C. Schroder, J.P. Schwarz, J.M. St.Clair, S.D. Steenrod, B.B. Stephens, S.A. Strode, C. Sweeney, D. Tanner, A.P. Teng, A.B. Thames, C.R. Thompson, K. Ullmann, P.R. Veres, N. Vieznor, N.L. Wagner, A. Watt, R. Weber, B. Weinzierl, P.O. Wennberg, C.J. Williamson, J.C. Wilson, G.M. Wolfe, C.T. Woods, and L.H. Zeng. **2018**. ATom: Merged Atmospheric Chemistry, Trace Gases, and Aerosols. ORNL DAAC, Oak Ridge, Tennessee, USA. https://doi.org/10.3334/ORNLDAAC/1581

AWARDS AND HONORS

UC Irvine Chemistry Teaching Assistant Mentor	2018
NASA Group Achievement Award for Participation in ATom	2019
National Center for Integration of Research, Teaching and Learning (CIRTL) Associate Level Certificate	2020
UCI DTEI Course Design Certificate	2020
UCI DTEI Certificate of Teaching Excellence	2020
NASA Group Achievement Award for Participation in FIREX-AQ	2020

ABSTRACT OF THE DISSERTATION

Global Observations of Oceanic Alkyl Nitrates and Dimethyl Sulfide during the NASA Atmospheric Tomography Mission (ATom)

By

Christopher Thomas Woods

Doctor of Philosophy in Chemistry

University of California, Irvine, 2020

Professor Donald R. Blake, Chair

Oceanic trace gases were measured onboard the NASA DC-8 flying laboratory during the NASA Atmospheric Tomography field campaign with the intent to examine the spatial and temporal fluctuations to the global distribution of these species, as well as establish a dataset of global background levels for future use in the validation of satellites and the constraint of chemical transport models. Airborne in situ measurements of VOCs were obtained via the UC Irvine whole air sampler (WAS) system and analyzed with gas chromatography/mass spectrometry.

The ATom mission was comprised of 4 deployments, each corresponding to the seasons. Each deployment, the NASA DC-8 flew a near circumnavigation of the earth, from 82 °N to 86 °S, while performing vertical soundings from 0.5-12.5 km in altitude. Flight paths over the Pacific, Atlantic and Southern Oceans allowed for the investigation of seasonal effects on anthropogenic and biogenic emissions in the remote atmosphere.

Alkyl nitrates ($RONO_2$) are an important source of reactive nitrogen to the remote atmosphere, where they can constitute the majority of the NO_y budget. In the Northern Hemisphere, C_2-C_5 nitrates are mostly generated photochemically. However, smaller carbon number alkyl nitrates (C_1-C_4) have a significant ocean source with spatial and temporal variability that are not fully understood. These 'light' alkyl nitrates were found to contribute up

to 88% of measured NO_y in the Southern Hemisphere marine boundary layer. Global measurements of $RONO_2$ showed enhancements at the equator and in the Southern Ocean, with seasonal maximums coinciding with conditions of increased marine biological productivity. $MeONO_2$ was the most abundant, with enhancements > 100 ppt at the equator, contributing a up to 77% of measured NO_y mixing ratios alone. Observations of 2-Butyl nitrate in the southern hemisphere marine boundary layer were shown to correlate with $MeONO_2$, suggesting an oceanic source unconsidered in recent literature.

Dimethyl Sulfide (DMS), another oceanic trace gas, is a by-product of marine biological production with impacts to short-wave forcing through incorporation into aerosol, causing direct and indirect radiative effects. In remote atmospheres, DMS may condense onto existing particles or participate in new particle formation: becoming a significant contributor to cloud condensation nuclei (CCN). Global observations of DMS in the boundary layer showed enhancements in the tropics (> 150 ppt), the Southern Ocean (>100 ppt) and the northern midlatitudes in the Atlantic (>100 ppt). Although, these increases in DMS production were not found to follow a consistent latitudinal gradient.

INTRODUCTION

1.1 Composition of the Atmosphere

The atmosphere is composed of four main gases: nitrogen, oxygen, argon, and water. While these gases make up 99.9% of the atmosphere, the species that make up the remaining fraction are part of complex dynamics in the earth system. Many of these so-called 'trace' gases are part of natural biogeochemical cycles, while others are anthropogenic or are enhanced above ambient levels by anthropogenic emissions. The dynamics of these gases are vital to our understanding of their impacts upon environmental and human health, climate change and the earth system.

1.2 Trace Gases Related to Climate Change

Gases that directly affect the radiative balance of the atmosphere by absorbing and reemitting infrared radiation (IR) are known as greenhouse gases. Radiative balance is also affected by altering the amount of light that surfaces reflect into space, a property known as albedo. Secondary products of VOC photochemistry can also become incorporated into particles, which has both direct and indirect effects to climate (Lohmann and Feichter, 2005).

1.2.1 Dimethyl Sulfide and Aerosol

Dimethyl sulfide (DMS) is a biogenic gas that affects climate feedbacks in the marine atmosphere. Due to its relatively short lifetime, ~1 day, (Barnard et al., 1982), DMS does not have large-scale effects in the gas phase. Upon emission into the atmosphere, DMS is oxidized to methanesulfonic acid (MSA) or sulfur dioxide (SO_2) (Figure 1.1) which can then by oxidized to sulfuric acid (H_2SO_4). MSA and H_2SO_4 are then available to incorporate into aerosol through various mechanisms (Andreae and Crutzen, 1997). In addition, data that were collected as a part of this work lead to the discovery of a previously unobserved DMS oxidation mechanism, in which hydroperoxymethyl thioformate (HPMTF) is formed. The subsequent HPMTF is available to incorporate into aerosol and functions as a major reservoir of marine sulfur (Veres et al., 2020). Particles formed from DMS have direct effects on local radiative forcing through

scattering, absorption and emission of radiation (Haywood and Boucher, 2000). DMS can also have indirect radiative effects by altering the properties and dynamics of clouds (Lohmann and Feichter, 2005). DMS products can form a subset of aerosol known as cloud condensation nuclei (CCN), which promote cloud formation. CCN form cloud droplets by lowering the vapor pressure of gaseous water (i.e. Kelvin effect), allowing the water to condense and form the types of water droplets found in clouds and fogs (Finlayson-Pitts and Pitts, 2000). In the remote atmosphere, especially near the poles, these CCNs can be sparse (Veres et al., 2020). As such, new particle formation due to DMS oxidation has powerful implications for cloud seeding, albedo and climate in the remote marine atmosphere (Gali et al., 2019).

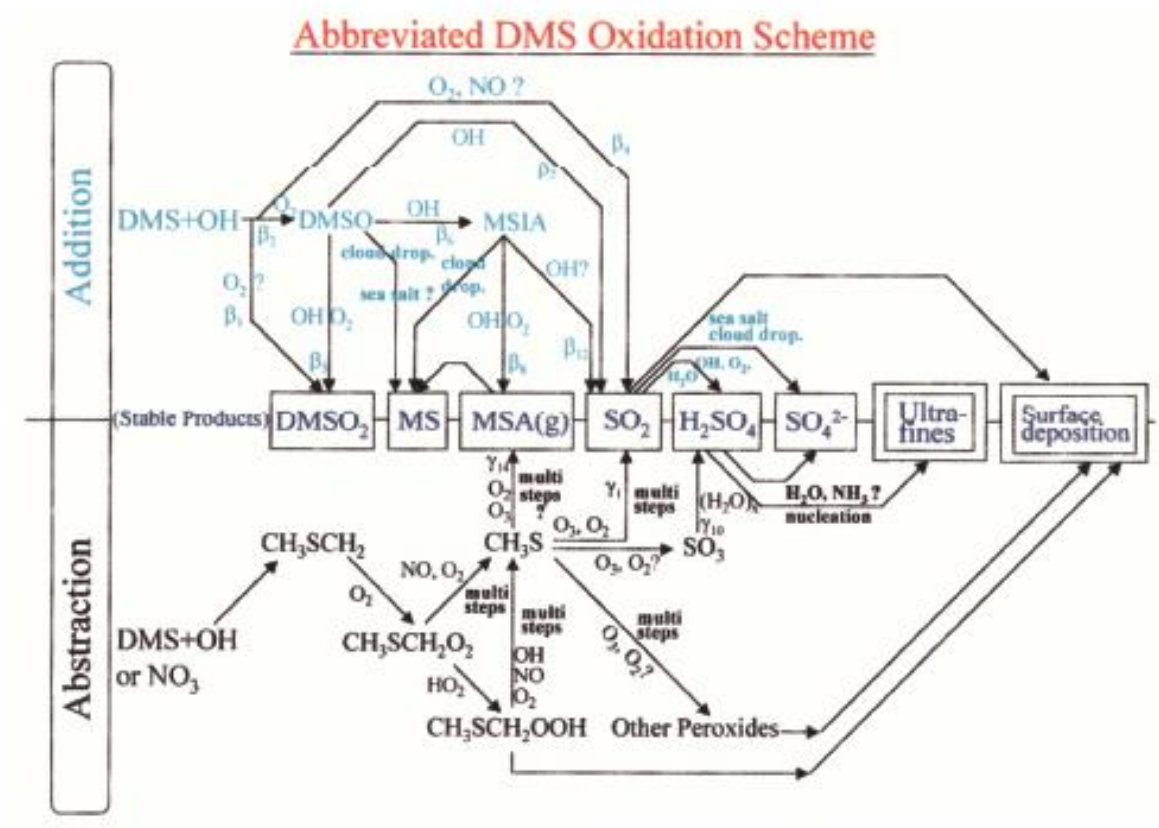

Figure 1.1 An abbreviated schematic of DMS oxidation. Chemical notation: DMSO, dimethyl sulfoxide; $DMSO_2$, dimethyl sulfone; MSIA, methane sulfinic acid; MSA(g), methanesulfonic acid; MSA(p) or MS, methane sulfonate. Adapted from Davis et al.(1999)

DMS is a product of the marine microbiome. Certain species of plankton emit a DMS precursor, dimethylsulfoniopropionate (DMSP), as part of their metabolism. DMSP is then consumed by bacteria, which emit DMS as a product (Andreae and Crutzen, 1997). Thus, DMS production is dependent on factors that affect these plankton populations (sea surface temperature, nutrient availability, etc.). Coral reefs are also significant sources of DMS, where DMSP is produced as part of the stress response and subsequently oxidized in surface waters or during coral air exposure (Hopkins et al., 2016). Of the total DMS dissolved in the surface ocean, only a fraction exchanges into the atmosphere as the process is heavily dependent on wind speed (Mahmood et al., 2019). However, the relationship between wind and DMS flux is nonlinear, as wind also affects DMS production by exerting controls on mixed layer depth, nutrient availability and sunlight penetration.

According to the CLAW hypothesis (named after the authors, Charlson, Lovelock, Andreae and Warren) DMS provides a negative climate feedback as increasing temperatures lead to higher DMS emissions, promoting CCN/cloud formation, which then lowers temperatures and suppresses DMS production (Charlson et al., 1987). After decades of research, it has been found that the relationship between DMS and CCN is more nuanced than the CLAW hypothesis states. Recent work has found that, on the global scale, the climate feedback provided by DMS is not impactful to climate change (Woodhouse et al., 2013). However, these effects have been found to be regionally important, especially in the arctic (Mahmood et al., 2019) and in areas populated with coral reef (Cropp et al., 2018) where DMS strongly influences aerosol and low clouds. In the Arctic, where warming is occurring faster, the melting of sea ice creates more ocean surface available for DMS production. In addition to the ocean, the higher latitudes of the Arctic contain non-marine sources of DMS that aren't fully accounted for, including lakes, coastal tundra and melt ponds on sea ice (Mungall et al., 2016).

DMS emission is sensitive to perturbations in biogeochemical cycles. Factors such as ocean acidification, as well as anthropogenic changes to the global marine N budget and

subsequent impacts on net primary production may have significant feedbacks on the biological production of DMS (Hopkins et al., 2020). The complexity and variability of marine DMS production leads to considerable uncertainty in the magnitude of its effects on climate as well as how this production will be affected by climate change.

1.3 Trace Gases Affecting Air Quality

Various gases can have adverse effects on air quality either directly (primary pollutants), or through their reaction products in the atmosphere (secondary pollutants). Ozone is a strong oxidant that is harmful to humans, animals, and plants. Ozone is also detrimental to air quality in the troposphere due to its role as the driver of photochemical smog formation (Finlayson-Pitts and Pitts, 2000). Ozone is generated in the troposphere through the products of VOC oxidation and oxides of nitrogen ($NO_x \equiv NO+NO_2$). It is primarily formed through the photolysis of NO_2 (reactions 1.1-2) Blacet(1952). Anthropogenic emissions of precursor species greatly enhance O_3 levels in polluted atmospheres.

$$NO_2 + h\nu \longrightarrow NO + O(^3P) \qquad (h\nu \leq 420 \text{ nm}) \qquad (1.1)$$

$$O(^3P) + O_2 \xrightarrow{M} O_3 \qquad (1.2)$$

1.3.1 Oxides of Nitrogen

NO_x is pivotal in generation of O_3 in the troposphere. However, NO_x has a relatively short atmospheric lifetime (< 12 hrs) in the troposphere (Liu et al., 2016). Several compounds, known as reactive nitrogen (NO_y, or odd nitrogen) act as reservoirs for NO_x, with atmospheric lifetimes that are sufficiently long to allow for long range transport (Chuck et al., 2002). NO_y is defined as all the reactive nitrogen compounds that release NO_x upon atmospheric degradation ($NO_y \equiv NO_x$, HNO_2, HNO_3, N_2O_5, HONO, PAN, alkyl nitrates ($RONO_2$), peroxyalkyl nitrates ($ROONO_2$), etc.). These compounds play an important role in regulating O_3 levels in the remote atmosphere, where NO_x levels are generally low.

1.4 Alkyl Nitrates

Alkyl nitrates are a reactive nitrogen compounds that have both oceanic and anthropogenic sources. In polluted air, alkyl nitrates are formed by the reaction of NO_x with alkyl peroxy radicals (reaction 1.5a). The branching ratio for the formation of $RONO_2$ is dependent on the carbon number of the parent alkane, with $RONO_2$ formation favoring higher molecular weight species (Atkinson et al., 1983). As such, lighter alkyl nitrates (i.e., C_1-C_3) have typically low photochemical yields (<3%) under atmospheric conditions (Atkinson et al., 1982). Additionally, alkenes and phenols can form multifunctional nitrates through reactions with NO_3 radical during nighttime (Perring et al., 2013).

$$RH + OH \rightarrow R^{\cdot} + H_2O \quad (1.3)$$

$$R^{\cdot} + O_2 \rightarrow + RO_2^{\cdot} \quad (1.4)$$

$$RO_2^{\cdot} + NO \rightarrow RONO_2 \quad (1.5a)$$

$$RO_2^{\cdot} + NO \rightarrow RO^{\cdot} + NO_2 \quad (1.5b)$$

Dahl et al.(2003) showed that a similar mechanism to reaction 1.5a can occur in seawater, with the source of NO coming from the photolysis of nitrite in the surface ocean (reaction 1.6). The alkyl peroxy radicals are photochemically generated (reaction 1.7) from colored dissolved organic matter (CDOM), a mixture of organic compounds (aromatic amino acids, lignin phenols, humic or fulvic substances) that is found in areas of marine biological productivity (Nelson and Siegel, 2013).

$$NO_2^- \xrightarrow{h\nu,\, H_2O} NO + OH + OH^- \quad (1.6)$$

$$CDOM \xrightarrow{h\nu,\, O_2} ROO^{\bullet} \quad (1.7)$$

Alkyl nitrates are removed from the atmosphere via two major pathways, photolysis, and reaction with OH radical. For smaller carbon number (C_1-C_5), photolysis is the dominant sink (reaction 1.8) However, for higher carbon number alkyl nitrates, reaction with OH radical becomes more competitive (reaction 1.9) (Clemitshaw et al., 1997).

$$RONO_2 + h\nu \rightarrow RO^{\cdot} + NO_2 \quad (h\nu < 340\ nm) \tag{1.8}$$

$$RONO_2 + OH \rightarrow OVOC + NO_2 \tag{1.9}$$

Both major sinks of monofunctional alkyl nitrates result in the release of NO_x, demonstrating the ability for alkyl nitrates to function as a reservoir for these compounds. Due to their atmospheric lifetimes (Table 1.1) alkyl nitrates can undergo long range transport, providing a source of NO_x to locations remote from the site of emission, regulating O_3 production in remote atmospheres (Chuck et al., 2002). However, the function of NO_y as a source/sink of NO_x is relative. Contrary to the remote atmosphere, the photochemical source of the lighter, longer-lived nitrates is most likely a net sink of NOx in urban outflows (Fisher et al., 2018).

Compound	Formula	Lifetime (days)	Reference
Methyl nitrate	CH_3ONO_2	26	*a*
Ethyl nitrate	$C_2H_5ONO_2$	14	*a*
i-Propyl nitrate	$C_3H_7ONO_2$	8.3	*a*
2-Butyl nitrate	$C_4H_9ONO_2$	7	*b*

Table 1.1 Atmospheric lifetimes of oceanic alkyl nitrates. Lifetimes are controlled by photolysis, with reaction rate to OH increasing with carbon number. Lifetimes are globally averaged values.

[a] Fisher et al.(2018), [b] Fischer et al.(2000)

1.5 Trace Gases Affecting Stratospheric Ozone

In contrast to the troposphere, where ozone is considered a pollutant, ozone in the stratosphere plays an important role for the planet by absorbing ultraviolet radiation that is harmful to life (McKenzie et al., 2011). Increased levels of UV are damaging to DNA and have been linked to increased skin cancer in humans, plant damage and other negative ecological effects.

$$O_2 + h\nu \rightarrow O + O \tag{1.8}$$

$$O + O_2 + M \rightarrow O_3 + M \tag{1.9}$$

$$O_3 + h\nu \rightarrow O_2 + O \quad (h\nu < 320\ nm) \tag{1.10}$$

$$O + O_3 \rightarrow 2O_2 \quad (1.11)$$

The undisturbed cycling of O_3 is described in the Chapman Mechanism (reaction 1.8 – 1.11, (Chapman, 1930)). However, increasing anthropogenic emissions of ozone depleting substances such as chlorofluorocarbons (CFCs) created a seasonal ozone hole over the Antarctic (Anderson et al., 1991). F. Sherwood Rowland and Mario Molina (1974) proposed a mechanism in which the halogen radicals from CFCs interrupt the Chapman mechanisms, leading to catalytic O_3 destruction in the stratosphere (reaction 1.12-1.14). This was later proved through in situ measurements made during the Airborne Arctic Ozone Experiment (AAOE) in 1987 (Anderson et al., 1991). Measurements from the flight, dubbed the 'smoking gun' showed a sharp increase in ClO (a chlorine radical reservoir) with a simultaneous decrease in O_3.

Where X = (Cl, Br, I, NO, HO)

$$X + O_3 \rightarrow XO + O_2 \quad (1.12)$$

$$XO + O \rightarrow X + O_2 \quad (1.13)$$

$$\text{net: } O_3 + O \rightarrow 2O_2 \quad (1.14)$$

Other source gases such as methane (CH_4) and nitrous oxide (N_2O) also have the potential to deplete stratospheric ozone, however these species have received less attention as their effects on decadal timescales are comparatively small (Portmann et al., 2012). ~10% of stratospheric N_2O reacts with $O(^1D)$ (reaction 1.17) to provide NO_x (and subsequently, NO_y), which can participate in reaction 1.12-1.13 to destroy ozone. While N_2O is the dominant source of NO_x in the stratosphere, troposphere to stratosphere transport (TST) of NO_y is also an important contributor to the overall NO_y budget in the lower stratosphere (Murphy et al., 1993). Currently, this NO_y entering the stratosphere is hypothesized to be predominately from lighting in the upper troposphere (Ko et al., 1986).

$$N_2O + h\nu \rightarrow N_2 + O(^1D) \quad (1.15)$$

$$N_2O + O(^1D) \rightarrow N_2 + O_2 \quad (1.16)$$

$$N_2O + O(^1D) \rightarrow 2NO \quad (1.17)$$

1.6 Objectives and Motivation for this Work

Anthropogenic emissions have impacts that extend into the remote atmosphere. In the age of anthropogenic climate change, understanding the dynamics of these processes is fundamental to the development of mitigation strategies and the formulation of accurate climate projections. Of these processes, those governing the dynamics of short-lived (decades) climate forcers such as CH_4 and O_3 are especially important, as reductions in these compounds provide effective strategies to reduce global warming and improve air quality (Wofsy et al., 2015). The NASA Atmospheric Tomography Mission (ATom) was designed to fill the gaps in the data regarding remote locations. ATom accomplished this through exhaustive vertical profiling over the Pacific and Atlantic Oceans, including polar regions.

Satellites are invaluable platforms to monitor these dynamics in across the globe but require robust in situ data for validation. Chemical models are important tools for understanding the earth system as well as predicting the effects of perturbations and mitigation strategies on climate. However, these models need to be calibrated with real-world, up to date data. Until recently, scientists relied on a mixture of airborne/ shipborne campaigns and ground sites to provide this data, but none has had the spatial and temporal range necessary to take an in situ 'image' of the remote troposphere. ATom provides this breadth of coverage through its flight plan and payload of instruments measuring a suite of gases (VOC, GHGs, reactive nitrogen species, photoproducts, ozone depleting substances,) aerosols (secondary, sea-salt, black carbon, CCN), meteorological data and solar radiation data. The dataset provides unprecedented measurements of atmospheric background that may prove invaluable not only for understanding atmospheric properties in the current day, but also as baseline to investigate global change in the future.

While the design of ATom emphasizes the study of anthropogenic emissions, it is imperative to apply the same approach in the study of biogenic compounds. This is especially true with regards to how the sources/sinks of biogenic compounds are affected by climate

change, as well as how these substances interact with anthropogenic emissions in both urban and remote atmospheres. While there have been several airborne campaigns that have included measurements of oceanic alkyl nitrates and DMS (Blake et al., 2003; Atlas, 1988; Atlas, 2013), none had the spatial and temporal range necessary to investigate seasonal emissions spanning the Pacific and Atlantic Oceans.

This work seeks to examine the global distribution and seasonal trends of oceanic trace gases (DMS and alkyl nitrates) observed during ATom, as well as investigate potential impacts to the remote atmosphere. In chapter 3 of this work, seasonal effects and latitudinal trends of alkyl nitrates are probed, in addition to the potential for alkyl nitrates to be a source of NO_y to the lowermost stratosphere via tropical troposphere to stratosphere transport (TST). Chapter 4 presents a similar analysis for DMS measurements taken during ATom, including their global distribution, potential effects from climate change and connection to aerosol in the remote marine boundary layer.

REFERENCES

1. Lohmann, U.; Feichter, J., Global indirect aerosol effects: a review. *Atmospheric Chemistry and Physics* **2005,** *5*, 715-737.

2. Barnard, W. R.; Andreae, M. O.; Watkins, W. E.; Bingemer, H.; Georgii, H.-W., The flux of dimethylsulfide from the oceans to the atmosphere. *Journal of Geophysical Research: Oceans* **1982,** *87* (C11), 8787-8793.

3. Andreae, M. O.; Crutzen, P. J., Atmospheric aerosols: Biogeochemical sources and role in atmospheric chemistry. *Science* **1997,** *276* (5315), 1052-1058.

4. Veres, P. R.; Neuman, J. A.; Bertram, T. H.; Assaf, E.; Wolfe, G. M.; Williamson, C. J.; Weinzierl, B.; Tilmes, S.; Thompson, C. R.; Thames, A. B.; Schroder, J. C.; Saiz-Lopez, A.; Rollins, A. W.; Roberts, J. M.; Price, D.; Peischl, J.; Nault, B. A.; Moller, K. H.; Miller, D. O.; Meinardi, S.; Li, Q. Y.; Lamarque, J. F.; Kupc, A.; Kjaergaard, H. G.; Kinnison, D.; Jimenez, J. L.; Jernigan, C. M.; Hornbrook, R. S.; Hills, A.; Dollner, M.; Day, D. A.; Cuevas, C. A.; Campuzano-Jost, P.; Burkholder, J.; Bui, T. P.; Brune, W. H.; Brown, S. S.; Brock, C. A.; Bourgeois, I.; Blake, D. R.; Apel, E. C.; Ryerson, T. B., Global airborne sampling reveals a previously unobserved dimethyl sulfide oxidation mechanism in the marine atmosphere. *Proc. Natl. Acad. Sci. U. S. A.* **2020,** *117* (9), 4505-4510.

5. Haywood, J.; Boucher, O., Estimates of the direct and indirect radiative forcing due to tropospheric aerosols: A review. *Rev. Geophys.* **2000,** *38* (4), 513-543.

6. Finlayson-Pitts, B. J.; Pitts, J. A., *Chemistry Of The Upper and Lower Atmosphere*. Academic Press: San Diego, 2000.

7. Gali, M.; Devred, E.; Babin, M.; Levasseur, M., Decadal increase in Arctic dimethylsulfide emission. *Proc. Natl. Acad. Sci. U. S. A.* **2019,** *116* (39), 19311-19317.

8. Davis, D.; Chen, G.; Bandy, A.; Thornton, D.; Eisele, F.; Mauldin, L.; Tanner, D.; Lenschow, D.; Fuelberg, H.; Huebert, B.; Heath, J.; Clarke, A.; Blake, D., Dimethyl sulfide oxidation in the equatorial Pacific: Comparison of model simulations with field observations for DMS, SO2, H2SO4(g), MSA(g), MS and NSS. *Journal of Geophysical Research: Atmospheres* **1999,** *104* (D5), 5765-5784.

9. Hopkins, F. E.; Bell, T. G.; Yang, M. X.; Suggett, D. J.; Steinke, M., Air exposure of coral is a significant source of dimethylsulfide (DMS) to the atmosphere. *Scientific Reports* **2016,** *6*.

10. Mahmood, R.; von Salzen, K.; Norman, A. L.; Gali, M.; Levasseur, M., Sensitivity of Arctic sulfate aerosol and clouds to changes in future surface seawater dimethylsulfide concentrations. *Atmospheric Chemistry and Physics* **2019,** *19* (9), 6419-6435.

11. Charlson, R. J.; Lovelock, J. E.; Andreae, M. O.; Warren, S. G., OCEANIC PHYTOPLANKTON, ATMOSPHERIC SULFUR, CLOUD ALBEDO AND CLIMATE. *Nature* **1987,** *326* (6114), 655-661.

12. Woodhouse, M. T.; Mann, G. W.; Carslaw, K. S.; Boucher, O., Sensitivity of cloud condensation nuclei to regional changes in dimethyl-sulphide emissions. *Atmospheric Chemistry and Physics* **2013,** *13* (5), 2723-2733.

13. Cropp, R.; Gabric, A.; van Tran, D.; Jones, G.; Swan, H.; Butler, H., Coral reef aerosol emissions in response to irradiance stress in the Great Barrier Reef, Australia. *Ambio* **2018,** *47* (6), 671-681.

14. Mungall, E. L.; Croft, B.; Lizotte, M.; Thomas, J. L.; Murphy, J. G.; Levasseur, M.; Martin, R. V.; Wentzell, J. J. B.; Liggio, J.; Abbatt, J. P. D., Dimethyl sulfide in the summertime Arctic atmosphere: measurements and source sensitivity simulations. *Atmospheric Chemistry and Physics* **2016,** *16* (11), 6665-6680.

15. Hopkins, F. E.; Suntharalingam, P.; Gehlen, M.; Andrews, O.; Archer, S. D.; Bopp, L.; Buitenhuis, E.; Dadou, I.; Duce, R.; Goris, N.; Jickells, T.; Johnson, M.; Keng, F.; Law, C. S.; Lee, K.; Liss, P. S.; Lizotte, M.; Malin, G.; Murrell, J. C.; Naik, H.; Rees, A. P.; Schwinger, J.; Williamson, P., The impacts of ocean acidification on marine trace gases and the implications for atmospheric chemistry and climate. *Proc. R. Soc. A-Math. Phys. Eng. Sci.* **2020,** *476* (2237), 35.

16. Blacet, F. E., Photochemistry in the Lower Atmosphere. *Industrial & Engineering Chemistry* **1952,** *44* (6), 1339-1342.

17. Liu, F.; Beirle, S.; Zhang, Q.; Doerner, S.; He, K.; Wagner, T., NOx lifetimes and emissions of cities and power plants in polluted background estimated by satellite observations. *Atmospheric Chemistry and Physics* **2016,** *16* (8), 5283-5298.

18. Chuck, A. L.; Turner, S. M.; Liss, P. S., Direct evidence for a marine source of C-1 and C-2 alkyl nitrates. *Science* **2002,** *297* (5584), 1151-1154.

19. Atkinson, R.; Carter, W. P. L.; Winer, A. M., EFFECTS OF TEMPERATURE AND PRESSURE ON ALKYL NITRATE YIELDS IN THE NOX PHOTOOXIDATIONS OF NORMAL-PENTANE AND NORMAL-HEPTANE. *Journal of Physical Chemistry* **1983,** *87* (11), 2012-2018.

20. Atkinson, R.; Aschmann, S. M.; Carter, W. P. L.; Winer, A. M., Kinetics of the gas-phase reactions of OH radicals with alkyl nitrates at 299 ± 2 K. *International Journal of Chemical Kinetics* **1982,** *14* (8), 919-926.

21. Perring, A. E.; Pusede, S. E.; Cohen, R. C., An Observational Perspective on the Atmospheric Impacts of Alkyl and Multifunctional Nitrates on Ozone and Secondary Organic Aerosol. *Chemical Reviews* **2013,** *113* (8), 5848-5870.

22. Dahl, E. E.; Saltzman, E. S.; de Bruyn, W. J., The aqueous phase yield of alkyl nitrates from ROO+NO: Implications for photochemical production in seawater. *Geophys. Res. Lett.* **2003,** *30* (6).

23. Nelson, N. B.; Siegel, D. A., The global distribution and dynamics of chromophoric dissolved organic matter. *Annual review of marine science* **2013,** *5*, 447-476.

24. Clemitshaw, K. C.; Williams, J.; Rattigan, O. V.; Shallcross, D. E.; Law, K. S.; Cox, R. A., Gas-phase ultraviolet absorption cross-sections and atmospheric lifetimes of several C-2-C-5 alkyl nitrates. *Journal of Photochemistry and Photobiology a-Chemistry* **1997,** *102* (2-3), 117-126.

25. Fisher, J. A.; Atlas, E. L.; Barletta, B.; Meinardi, S.; Blake, D. R.; Thompson, C. R.; Ryerson, T. B.; Peischl, J.; Tzompa-Sosa, Z. A.; Murray, L. T., Methyl, Ethyl, and Propyl Nitrates: Global Distribution and Impacts on Reactive Nitrogen in Remote Marine Environments. *J. Geophys. Res.-Atmos.* **2018,** *123* (21), 12429-12451.

26. Fischer, R. G.; Kastler, J.; Ballschmiter, K., Levels and pattern of alkyl nitrates, multifunctional alkyl nitrates, and halocarbons in the air over the Atlantic Ocean. *J. Geophys. Res.-Atmos.* **2000,** *105* (D11), 14473-14494.

27. McKenzie, R. L.; Aucamp, P. J.; Bais, A. F.; Björn, L. O.; Ilyas, M.; Madronich, S., Ozone depletion and climate change: impacts on UV radiation. *Photochemical & Photobiological Sciences* **2011,** *10* (2), 182-198.

28. Chapman, S., XXXV. On ozone and atomic oxygen in the upper atmosphere. *The London, Edinburgh, and Dublin Philosophical Magazine and Journal of Science* **1930,** *10* (64), 369-383.

29. Anderson, J. G.; Toohey, D.; Brune, W. H., Free radicals within the Antarctic vortex: The role of CFCs in Antarctic ozone loss. *Science* **1991,** *251* (4989), 39-46.

30. Molina, M. J.; Rowland, F. S., STRATOSPHERIC SINK FOR CHLOROFLUOROMETHANES - CHLORINE ATOMIC-CATALYSED DESTRUCTION OF OZONE. *Nature* **1974,** *249* (5460), 810-812.

31. Portmann, R.; Daniel, J.; Ravishankara, A., Stratospheric ozone depletion due to nitrous oxide: influences of other gases. *Philosophical Transactions of the Royal Society B: Biological Sciences* **2012,** *367* (1593), 1256-1264.

32. Murphy, D. M.; Fahey, D. W.; Proffitt, M. H.; Liu, S. C.; Chan, K. R.; Eubank, C. S.; Kawa, S. R.; Kelly, K. K., REACTIVE NITROGEN AND ITS CORRELATION WITH OZONE IN THE LOWER STRATOSPHERE AND UPPER TROPOSPHERE. *J. Geophys. Res.-Atmos.* **1993,** *98* (D5), 8751-8773.

33. Ko, M. K. W.; McElroy, M. B.; Weisenstein, D. K.; Sze, N. D., LIGHTNING - A POSSIBLE SOURCE OF STRATOSPHERIC ODD NITROGEN. *J. Geophys. Res.-Atmos.* **1986,** *91* (D5), 5395-5404.

34. Wofsy, S. C.; Prather, M. J.; Ryerson, T. B.; Newman, P., Atmospheric Tomography Mission (ATom) Executive Summary. 2015.

35. Blake, N. J.; Blake, D. R.; Swanson, A. L.; Atlas, E.; Flocke, F.; Rowland, F. S., Latitudinal, vertical, and seasonal variations of C-1-C-4 alkyl nitrates in the troposphere over the Pacific Ocean during PEM-Tropics A and B: Oceanic and continental sources. *J. Geophys. Res.-Atmos.* **2003,** *108* (D2).

36. Atlas, E., EVIDENCE FOR GREATER-THAN-OR-EQUAL-TO-C-3 ALKYL NITRATES IN RURAL AND REMOTE ATMOSPHERES. *Nature* **1988,** *331* (6155), 426-428.

37. Atlas, E., HIPPO Merged GC WAS. Version 1.0. ed.; UCAR/NCAR -Earth Observing Laboratory: 2013.

CHAPTER 2

EXPERIMENTAL METHODS

2.1 Whole Air Sampling Approach

The Rowland-Blake group collects samples for trace gas analysis via a whole-air sampling methodology. Whole-air samples were collected on site using proprietary evacuated stainless-steel canisters. Upon collection, sample canisters are transported back to the lab at UC Irvine to undergo analysis via gas chromatography.

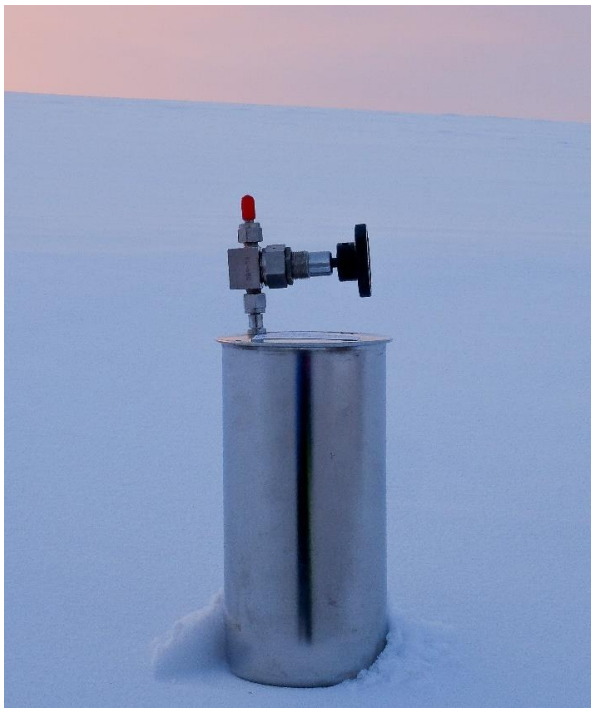

Figure 2.1 Whole air sampling canister, with valve installed

2.2 Canister Description and Preparation

Sample canisters (Figure 2.1) were constructed previously from two pieces: a ported top and a cylindrical body (Sive, 1998). The parts were electropolished before assembly by welding. The approximate volume of each canister is ~ 2 liters and are operated by a Swagelok valve installed on the port. Before use, cans were baked for 24 hours at 160°C and then underwent

several cycles pumping and flushing with compressed air and helium. Depending on end use, cans had 17 torr of water vapor added to passivate the interior surface.

For airborne operations, sets of 24 canisters were secured in high density foam, configured in 3 rows of 8 and plumbed together in series with 1/4-inch O.D. stainless-steel tubing using ultra torr fittings. The 3 lines were connected with stainless steel flex tubing, creating one continuous line that includes each canister in a zig-zag pattern. The complete unit is affectionately known as a “snake” (Figure 2.2).

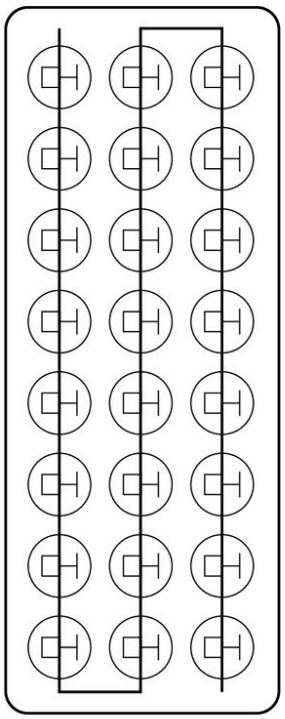

Figure 2.2 A sample “Snake”, holding 24 sample canisters inside a foam carton.

2.3 Land Sampling Protocol

When sampling at ground level, the protective cap was removed from the valve and the air from that headspace was flushed with the air of the sample location. All sampling was performed with the operator and canister valve opening oriented towards the wind. Canisters were opened slowly so that the rate of fill was consistent, with the total sampling time of 45-60 seconds. To prevent can-to-air exchange, the valves were closed just before pressure is equilibrated and the protective cap replaced.

2.4 Aircraft Sampling Protocol

Operating the Whole Air Sampler (WAS) aboard aircraft is a dynamic process that required certain considerations based on aircraft platform, altitude, area of operations and a host of other factors. Below is the description of the setup used aboard the NASA McDonnell Douglas DC-8 aircraft, the platform used for the Atom campaign.

2.4.1 Payload

Aboard the DC-8, the WAS station consisted of two metal racks, each containing 4 vertical bays. Each bay housed one snake, for a maximum capacity of 7 snakes (168 canisters) per research flight. The remaining bay contained a twin bellows compressor (connected in series) and power supply. The fore rack was fitted with a manifold that connects the sample inlet (0.25”, installed on the fuselage exterior) to the pump, snake inlets and outlets. This manifold was also connected to the aft rack in a manner such that each snake and rack are isolable to each other and to the flow of air coming from the sample inlet/pump/outlet stream. A low-pressure gas tank was also affixed to the aft rack exterior. This tank was filled by the pump in-flight with outside air. Between flights, this tank was used to perform leak checks, as well as 10-minute flushes of the snake/manifold lines to ensure the displacement of any cabin air in the lines.

2.4.2 Canister Sampling

Shortly after takeoff, the line was primed by pumping 0 ~20 psig and flushing several times. To take a sample, the snake outlet was closed allowing the line to build pressure. The sample valve was then opened slowly, maintaining positive line pressure, to ensure the vacuum suction did not pull cabin air into the sample. All samples were filled to ~30 psig before the valves were closed and the line pressure released via the outlet valve. Sample order within a snake was perpendicular to the plumbing order, to minimize systematic error.

2.4.3 Special Considerations

Airborne measurements are made in a vast variety of conditions. Warm, humid air below the boundary layer in the tropics poses different challenges to cold, dry air at 12 km of altitude.

For colder, dryer conditions, a heated inlet was used to prevent sticking of less volatile gases. In addition, due to the mechanical limitations of the bellows pump, samples taken near the DC-8's operational ceiling took a factor of 2-3 longer to fill than samples at lower altitudes.

2.5 NMHC Gas Chromatograph System

After collection, samples were shipped back to UC Irvine for analysis. Samples were preconcentrated and analyzed for trace gases with a suite of complimentary gas chromatographs (GC).

2.5.1 The Manifold

The manifold for loading, concentrating/trapping and finally injecting gaseous sample was constructed according to Figure 2.3. Internal pressure was monitored by thermocouple and capacitance manometer. For pressurized samples, an "excess canister" was used to measure out precise sample amount. The sample trap consisted of a 1/4-inch stainless-steel loop, filled with 3 mm glass beads, with a total approximate volume of 10 mL. Glass vacuum flasks containing liquid nitrogen or near-boiling water were used respectively to immerse the loop for trapping or revolatilizing target gas species. A flow controller was installed upstream of the trap to monitor flow. Two mechanical pumps were used to evacuate the lines. Ultrapure helium was used to flush the trap between injections.

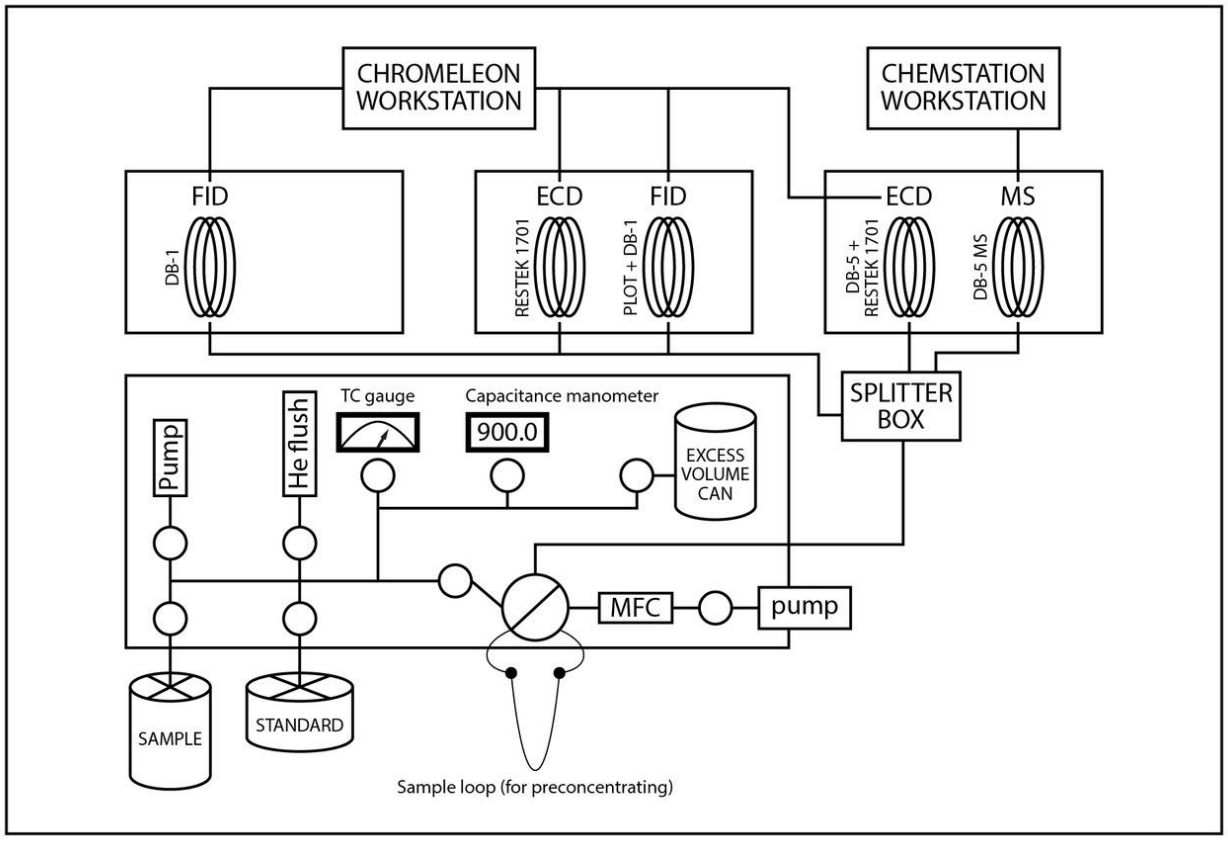

Figure 2.3 Schematic of the UCI NMHC manifold and GC array

2.5.2 Sample Loading Protocol

Before trapping a sample, ultrapure helium was sucked through the loop for 1 minute at a flow rate of 500 cm^3/min. The sample trap was then cooled for 2 minutes in liquid nitrogen before trapping. For ground-based samples, or samples that were at ambient pressure, samples were sucked through the trap directly from the canister. For pressurized samples, 1000.0 torr of sample was transferred to the evacuated excess can, from which 900.0 torr of sample was sucked through the trap. The sample loop remained on vacuum for 1 minute to remove any additional oxygen before being isolated via the switching valve. Samples were then revolatilized by immersing the loop in near-boiling water before being injected into the system.

2.5.3 Standards

A mixture containing 67 gases was made in-house and used as an internal standard to measure response factors, as well as monitor system performance. Standards were made from

air that was collected at White Mountain Research Station (WMRS, altitude 10,200 feet), a remote, atmospherically clean location in the eastern Sierra Nevada Mountains. To this air, a mixture of additional gases was added and the standard calibrated to a historical standard. A subset of these gases, the alkyl nitrate species, were calibrated separately by the Elliot Atlas Group at the University of Miami. Standards were loaded/trapped for analysis using the same procedure as samples, with the exception that 2.0 torr of water vapor were added to the excess can, prior to trapping. Standards were run after every eight samples.

2.5.4 Gas Chromatograph Systems

Injected sample ran through a house-made splitter, sending it to an array of three GC's. All three were equipped with liquid nitrogen cryogenic valves and attached to a shared liquid N_2 supply system. The details of which are as follows.

2.5.4.1 Gas Chromatographs

The system consisted of 3 gas chromatographs: two Hewitt-Packard 6890 GCs and an Agilent 6890 GC/MS, attached in parallel to the sample injection line via a house-made splitter.

2.5.4.2 GC Capillary Columns

An array of capillary columns was used to resolve our large catalog of quantified compounds. Column information is summarized in Table 2.1. A DB-1 column attached to a flame ionization detector (FID) was used to measure C_3-C_{10} hydrocarbons. A Restek 1701 column connected to an ECD was used to measure alkyl nitrates and hydrocarbons. A DB-5MS column attached to an HP 5973 Quadrupole Mass Spectrometer (MS) was used to measure oxygenates. A DB-5 column followed by a Restek 1701 column connected in series to an electron capture detector (ECD) was also used to detect alkyl nitrates and halocarbons. In addition, a GS alumina PLOT column followed by a DB-1 column attached in series to an FID measured C_2-C_7 hydrocarbons.

Table 2.1 Column-detector combinations for GC array.

GC Name	Column Name	Column Type	Detector	Compounds
2	B	DB-1	FID	C_3-C_{10} hydrocarbons
GCMS	C	DB-5M + Restek 1701	MS/ECD	alkyl nitrates and hydrocarbons
	MS	DB-5MS	MS	oxygenates
3	D	Restek 1701	ECD	alkyl nitrates and hydrocarbons
	E	GS Alumina PLOT + DB-1	FID	C_2-C_7 hydrocarbons

2.5.4.3 Detectors

A series of detectors was used to obtain redundant measurements of a variety of VOCs. Each of the columns was mated to a flame ionization detector, electron capture detector or HP 5973 Quadrupole Mass Selective Detector. The column/detector assignments are displayed in Table 2.2.

2.5.4.4 Instrument Methods

Instruments were connected to PC via a universal GC serial connection hub. The GC's were programmed and operated using Chromeleon 6th edition software. The MS detector was operated with Agilent Chemstation software.

2.6 Data Post-Processing

Peak assignments and integration were semi-automated by the execution of a data processing method inside the GC software. While the Rowland-Blake group NMHC system is capable of measuring ~ 150 compounds, the compounds for which data were published during

the Atom campaign are as follows. A complete list of compounds was published by Colman et al.(2001)

Table 2.2 Compounds measured by UCI WAS for ATom Campaign. All values provided by Colman et al.(2001) unless otherwise noted.

	Compound	Formula	LOD (ppt)	Precision (%)	Accuracy (%)
Alkanes	Ethane	C_2H_6	3	1	5
	Propane	C_3H_8	3	2	5
	i-Butane	C_4H_{10}	3	3	5
	n-Butane	C_4H_{10}	3	3	5
	i-Pentane	C_5H_{12}	3	3	5
	n-Pentane	C_5H_{12}	3	3	5
	n-Hexane	C_6H_{14}	3	3	5
	n-Heptane	C_7H_{16}	3	3	5
	2-Methylpentane	C_6H_{14}	3	3	5
	3-Methylpentane	C_6H_{14}	3	3	5
Alkenes, Alkynes	Ethene	C_2H_4	3	3	5
	Ethyne	C_2H_2	3	3	5
	Propene	C_3H_6	3	3	5
	Isoprene	C_5H_8	3	3	5
Aromatics	Benzene	C_6H_6	3	3	5
	Toluene	C_7H_9	3	3	5
	Ethylbenzene	C_8H_{10}	3	3	5
	m/p-xylene	C_8H_{10}	3	3	5
	o-xylene	C_8H_{10}	3	3	5
Alkyl Nitrates	$MeONO_2$	CH_3ONO_2	0.02	5	10
	$EtONO_2$	$C_2H_5ONO_2$	0.02	5	10
	i-$PropONO_2$	$C_3H_7ONO_2$	0.02	5	10
	n-$PropONO_2$	$C_3H_7ONO_3$	0.02	5	10
	2-$BuONO_2$	$C_4H_9ONO_2$	0.02	5	10
	2-$PeONO_2$	$C_5H_{11}ONO_2$	0.02	5	10
	3-$PeONO_2$	$C_5H_{11}ONO_2$	0.02	5	10
	3-Methyl-2-$BuONO_2$	$C_5H_{11}ONO_2$	0.02	5	10
CFCs	CFC-11	CCl_3F	10	1	3
	CFC-12	CCl_2F_2	10	1	3

Table 2.2 continued

CFCs	CFC-113	CCl_2FCClF_2	5	1	3
	CFC-114	$CClF_2CClF_2$	1	1	5
HFCs	HFC-152a	$C_2H_4F_2$	[a]—	—	—
	HFC-134a	CH_2FCF_3	1	5.2	4.8
	HFC-365mfc	$CH_3CF_2CH_2CF_3$	—	—	—
HCFCs	HCFC-124	$CHClFCF_3$	—	—	—
	HCFC-22	CHF_2Cl	2	5	5
	HCFC-141b	CH_3CCl_2F	0.5	3	10
	HCFC-142b	CH_3CClF_2	0.5	3	10
Halons	Halon-1211	$CBrClF_2$	0.1	1	5
	Halon-1301	$CBrF_3$	0.1	10	5
	Halon-2402	$CBrF_2CBrF_2$	0.01	1	5
LLHCs	Methyl chloroform	CH_3CCl_3	0.1	5	5
	Carbon Tetrachloride	CCl_4	1	5	5
	Methyl Bromide	CH_3Br	50	5	10
	Methyl Chloride	CH_3Cl	0.5	5	10
VSLS	Bromoform	$CHBr_3$	0.01	10	20
	Dibromomethane	CH_2Br_2	0.01	5	20
	Bromodichloromethane	$CHBrCl_2$	0.01	10	50
	Dibromochloromethane	$CHBr_2Cl$	0.01	5	50
	Chloroform	$CHCl_3$	0.1	5	10
	Dichloromethane	CH_2Cl_2	1	5	10
	Tetrachloroethene	C_2Cl_4	0.01	5	10
	1,2-Dichloroethane	CH_2ClCH_2Cl	0.1	5	10
	Methyl Iodide	CH_3I	0.005	5	10
Sulfur Species	Carbonyl Sulfide	OCS	—	—	—
	Dimethyl Sulfide[b]	CH_3SCH_3	1	4	20

[a] denotes no data
[b] Simpson et al.(2001)

2.6.1 Data Modification

Excepting detectors with very high signal-to-noise, like the ECD, performance of software-automated peak integration was generally poor. Thus, each peak was manually

inspected and adjusted as needed to ensure correct peak assignment as well as bounds of integration.

2.7 NMHC System Performance during NASA ATom

Standards were used extensively to monitor performance and correct for any drift in columns or detectors that occurred over long periods of continuous sample analysis. Parent standards were run 1-2 times per day, while working standards were run every 3 hours. At the beginning of a continuous analysis session, a new curve monitoring standard response over time was begun for each gas species measurement from each detector. Any interruption in continuous sampling (i.e. instrument failure, logistics of shipping samples, etc.) would end the current period and begin a new curve. All samples within the run time/date interval of the curve were corrected for drift via the polynomial curve fit applied to each gas species for each detector. For example, inputting run time day 210.0 into the gas-specific equation gave the response factor for the concentration of said gas in the parent or running standard (~27,000 units). This could then be used to calculate mixing ratios for samples during this interval.

2.7.1 FID with PLOT Column

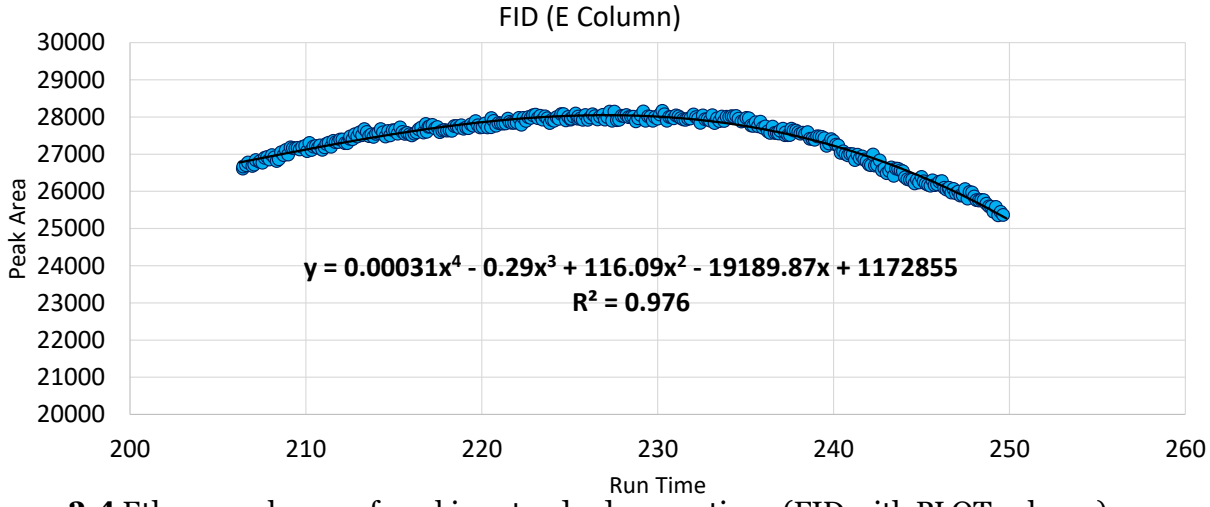

Figure 2.4 Ethane peak area of working standard vs run time, (FID with PLOT column) over ~40 days of 24/7 continuous sample analysis.

The first 30 days the whole air standard, which was analyzed every 3 hours, displayed an increasing detector sensitivity on the FID attached to the PLOT column (Figure 2.4) which peaked at about run day 237 and then drifted down for the remaining 15 days. Polynomial fit was applied to standard data to correct for FID drift (Blake, 2020). The analysis of working standards and parent standards was imperative to ensure data quality. This process was particularly important with the PLOT column, due to the tendency for larger molecular weight gases to stick to the column as it progresses in its service lifetime. This sticking produces smaller peaks in the chromatogram as the result of column degradation.

2.7.2 FID with DB-1 column

Figure 2.5 shows a more continuous trend for the peak area for ethylbenzene on a DB-1 column. In contrast to the PLOT, the DB-1 column exhibited a more predictable change in response over time. The decreasing trend in the area units of ethylbenzene (~25%) over the course of 20 continuous days could be detector response and/or column degradation.

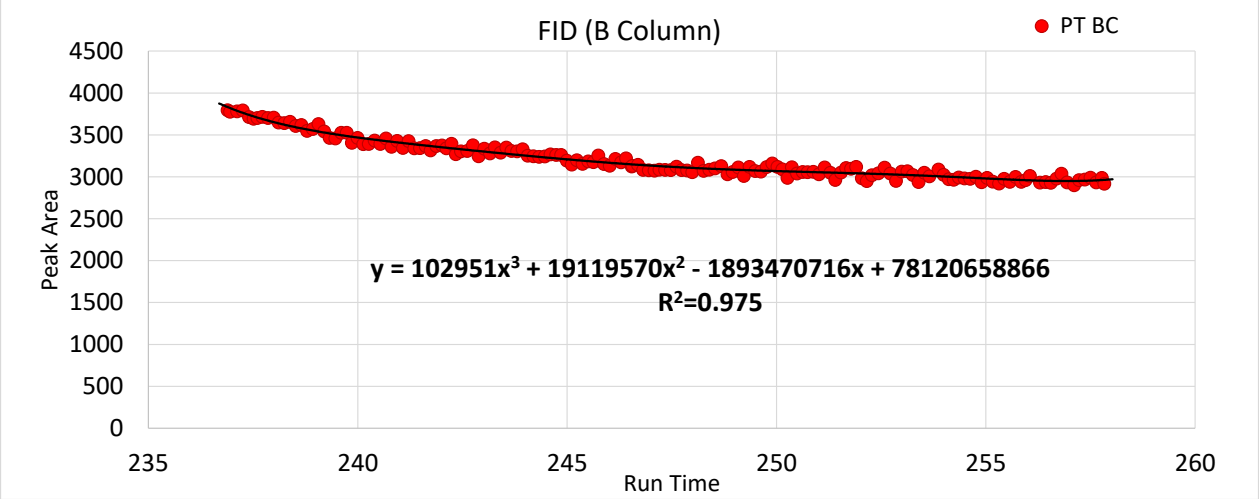

Figure 2.5 Ethylbenzene peak area of working standards vs run time, (FID with DB-1 column) over ~20 days of 24/7 continuous sample analysis.

2.7.3 MSD with DB-5MS column

The use of mass spectrometry for ambient air monitoring poses certain difficulties not encountered with other detectors. For a commercially available quadrupole MS, a filament provides the source of electrons, which thins over its life-cycle. Thinning of the filament results in fewer electrons being emitted by the filament and thus there are fewer electrons available to ionize the target molecules (Figure 2.6). For the FID in Figure 2.5, there were changes in sensitivity of 3800 to 3000 peak area, over a period of ~20 days (~1%/day). For the MS, a change in detector response of a factor of 5 was observed over the ~20 day period (at day 247, the filament failed and a new curve was recorded). This emphasizes the importance of running standards often and regularly are when using a mass-spec detector**.**

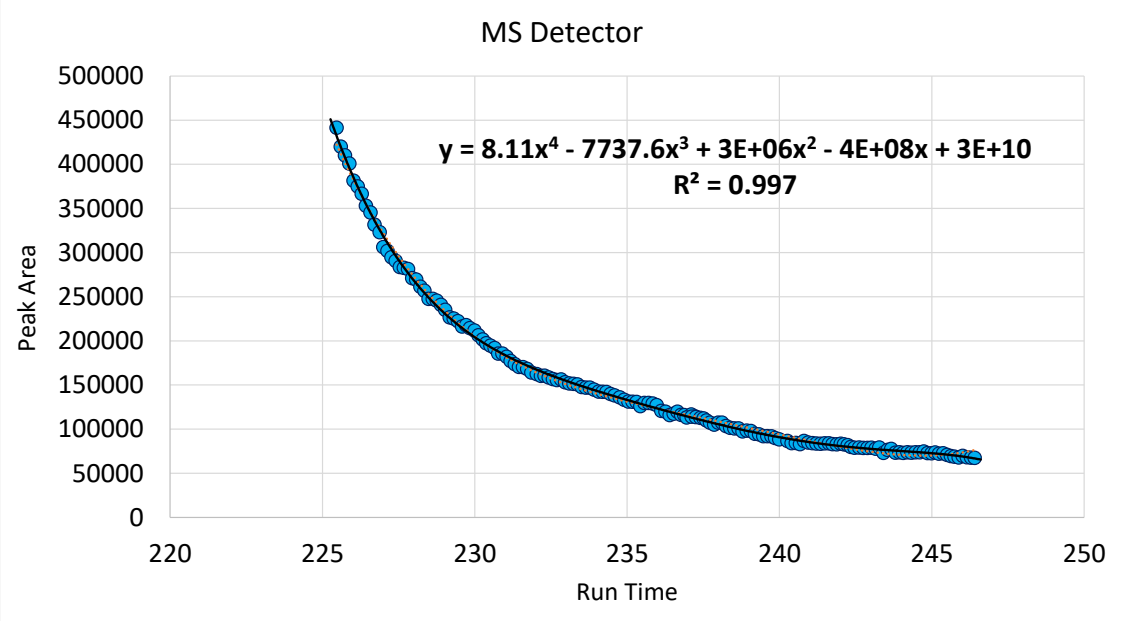

Figure 2.6 CFC-114 peak area of working standards vs run time, (MSD with DB-5MS column) over ~20 days of 24/7 continuous sample analysis

REFERENCES

1. Sive, B. C. Atmospheric Nonmethane Hydrocarbons: Analytical Methods and Estimated Hydroxyl Radical Concentrations. University of California, Irvine, 1998.

2. Colman, J. J.; Swanson, A. L.; Meinardi, S.; Sive, B. C.; Blake, D. R.; Rowland, F. S., Description of the analysis of a wide range of volatile organic compounds in whole air samples collected during PEM-Tropics A and B. *Anal. Chem.* **2001,** *73* (15), 3723-3731.

3. Simpson, I. J.; Colman, J. J.; Swanson, A. L.; Bandy, A. R.; Thornton, D. C.; Blake, D. R.; Rowland, F. S., Aircraft measurements of dimethyl sulfide (DMS) using a whole air sampling technique. *J. Atmos. Chem.* **2001,** *39* (2), 191-213.

4. Blake, D. R., UC Irvine, Personal communication, July 15, 2020.

CHAPTER 3

Alkyl Nitrates in The Remote Atmosphere During NASA ATom

This dissertation presents volatile organic compound (VOC) data collected aboard the NASA DC-8 research aircraft during the Atmospheric Tomography Mission (ATom). The ATom field campaign operated from July 2016 to May 2018 and was divided into four parts (Table 3.1).

Table 3.1 ATom deployment schedule

Deployment	Year	Flights	Season (Boreal)
ATom 1	2016	Jul 28 - Aug 22	Summer
ATom 2	2017	Jan 26 - Feb 25	Winter
ATom 3	2017	Sept 28 - Oct 23	Fall
ATom 4	2018	April 26- May 21	Spring

3.1 Campaign Design

ATom was designed to provide an exhaustive sounding of Earth's global background composition for use in calibrating satellites, constraining atmospheric models, and providing a baseline to monitor future change in the Earth System (Wofsy et al., 2015). The investigation was carried out using a general flight plan repeated in each of the four seasons. Each deployment was comprised of 11-13 research flights which together approximated a longitudinal circumnavigation of the Earth (Figure 3.1). Deployments began at Armstrong Flight Research Center in Palmdale, CA, where the NASA DC-8 is based. The first research flight consisted of a round trip from Palmdale to the equator to ensure the aircraft and instruments were fully operational. The DC-8 then flew north of the Arctic Circle and performed missed-approaches near Utqiagvik, Alaska. The following flights went south over the Pacific Ocean and

paused in Punta Arenas, Chile, where flights over Antarctica were conducted (during the last two ATom deployments). The northbound leg continued over the Atlantic Ocean to Greenland before heading back to the continental United States and finally transiting back to Palmdale.

Each flight featured a series of vertical profiles where the DC-8's altitude ranged between ~500 feet and up to 40,000 feet, capturing a global image of the boundary layer and free troposphere (Figure 3.2). Flight duration was generally 8-10 hours, operating primarily during daylight hours. Vertical profiles generally took ~1 hour of flight time, with an ascent/descent rate ~1500ft/min. Figure 3.3 shows the breakdown of typical flight legs during a deployment. Aboard the DC-8 was a suite of 24 instruments measuring aerosols, VOCs, OH radicals, black carbon and other physical and chemical atmospheric properties. Unlike more targeted airborne campaigns, routes were chosen specifically to avoid atmospheric chemical events such as smoke plumes, volcanic emissions, or urban emissions. However, these could not be completely avoided.

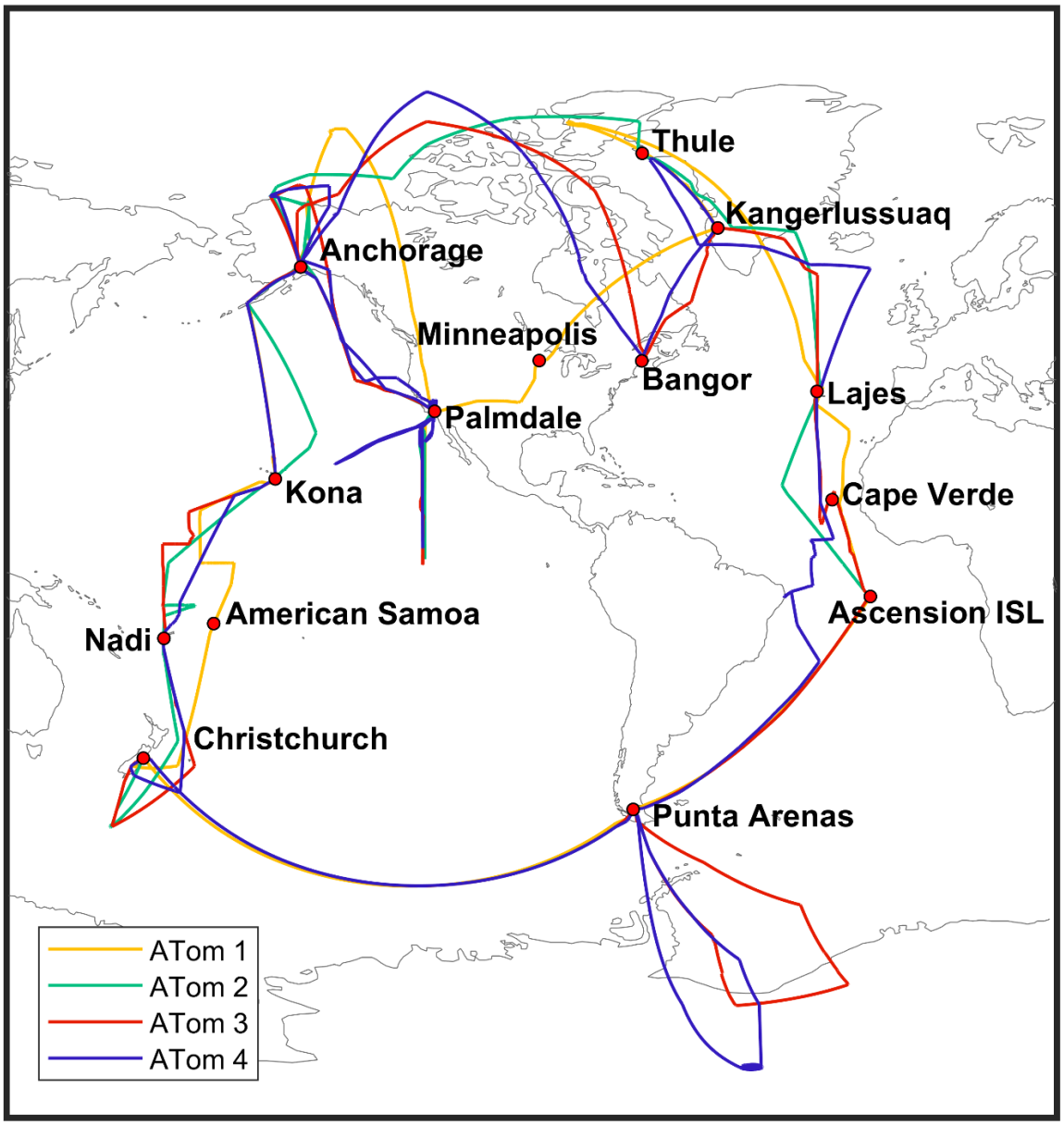

Figure 3.1 Map overview of the Atom campaign. Points represent airports visited on one or more deployments.

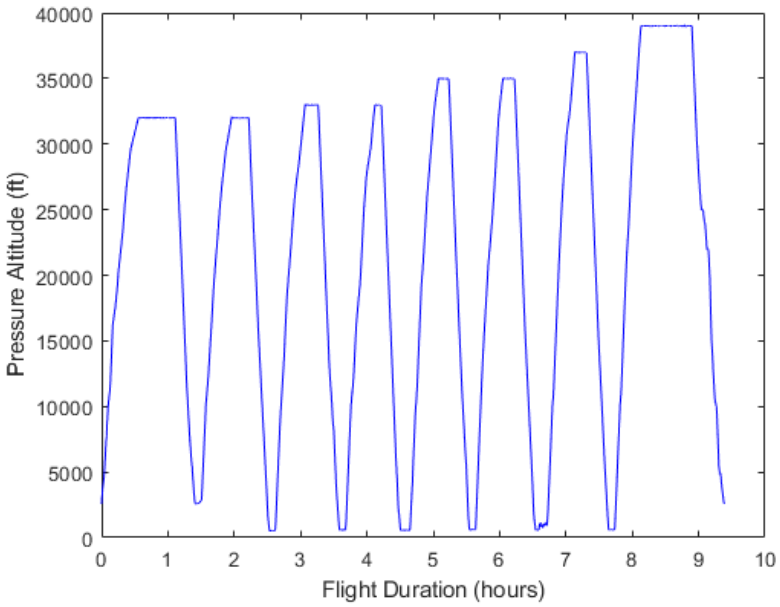

Figure 3.2 Example of a vertical profile taken during a round trip flight (ATom-2 Flight 1) to the equator.

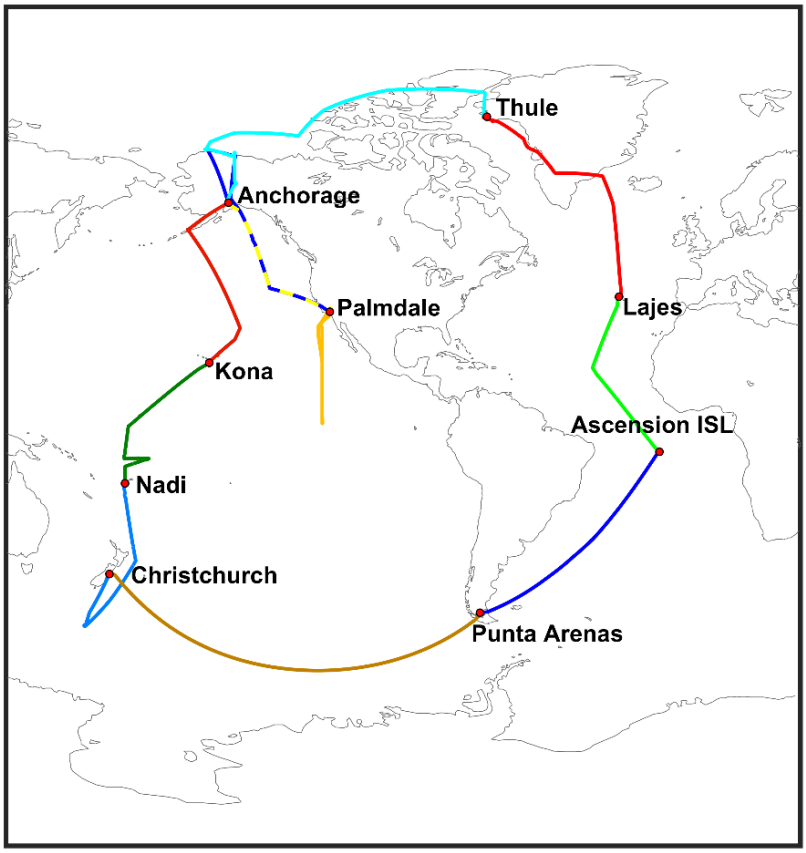

Figure 3.3 Example breakdown of an ATom deployment (ATom 2) where each color represents one research flight.

3.2 Global Distribution of C_1- C_5 Alkyl Nitrates

The ATom 2 deployment marked a maximum in the concentrations of many of the gases measured by UCI WAS. Here ATom 2 data are presented to depict the range of mixing ratios observed, as well as accentuate regional contrast. Figure 3.4 - 3.5 show the geographic distribution of methyl nitrate measured during each ATom deployment. Areas of increased methyl and ethyl nitrate mixing ratios were observed primarily over the oceans, though there were varying contributions from continental sources. In agreement with the literature, methyl and ethyl nitrate levels were found to be highest at the equator (Figure 3.6), where marine upwelling is strongest (Blake et al., 2003; Fisher et al., 2018). However, the strong ocean emissions were not constrained to the tropics. There were also consistent enhancements in the Southern Pacific Ocean, around 45°- 60° south, where $MeONO_2$ was found to contribute up to 77% of total NO_y mixing ratios. The vertical profiles depicted in Figure 3.7 show the low-altitude enhancements of methyl and ethyl nitrate in the tropics and Southern Ocean due to the ocean source. Excepting methyl nitrate, photochemical sources were the major contributors of alkyl nitrates in the northern extra-tropics. This can be seen especially in the C_3 - C_4 nitrates, where Figure 3.8 shows elevated mixing ratios of these species in the northern midlatitude boundary layer. Elevated levels of the C_5 nitrates were observed mainly in the northern hemisphere (Figure 3.9). Overall, contribution to NO_y by the C_1-C_4 nitrates was measured to be greatest in the Southern Pacific Ocean, where it was found to contribute up to 88% of the total NO_y mixing ratios in the boundary layer.

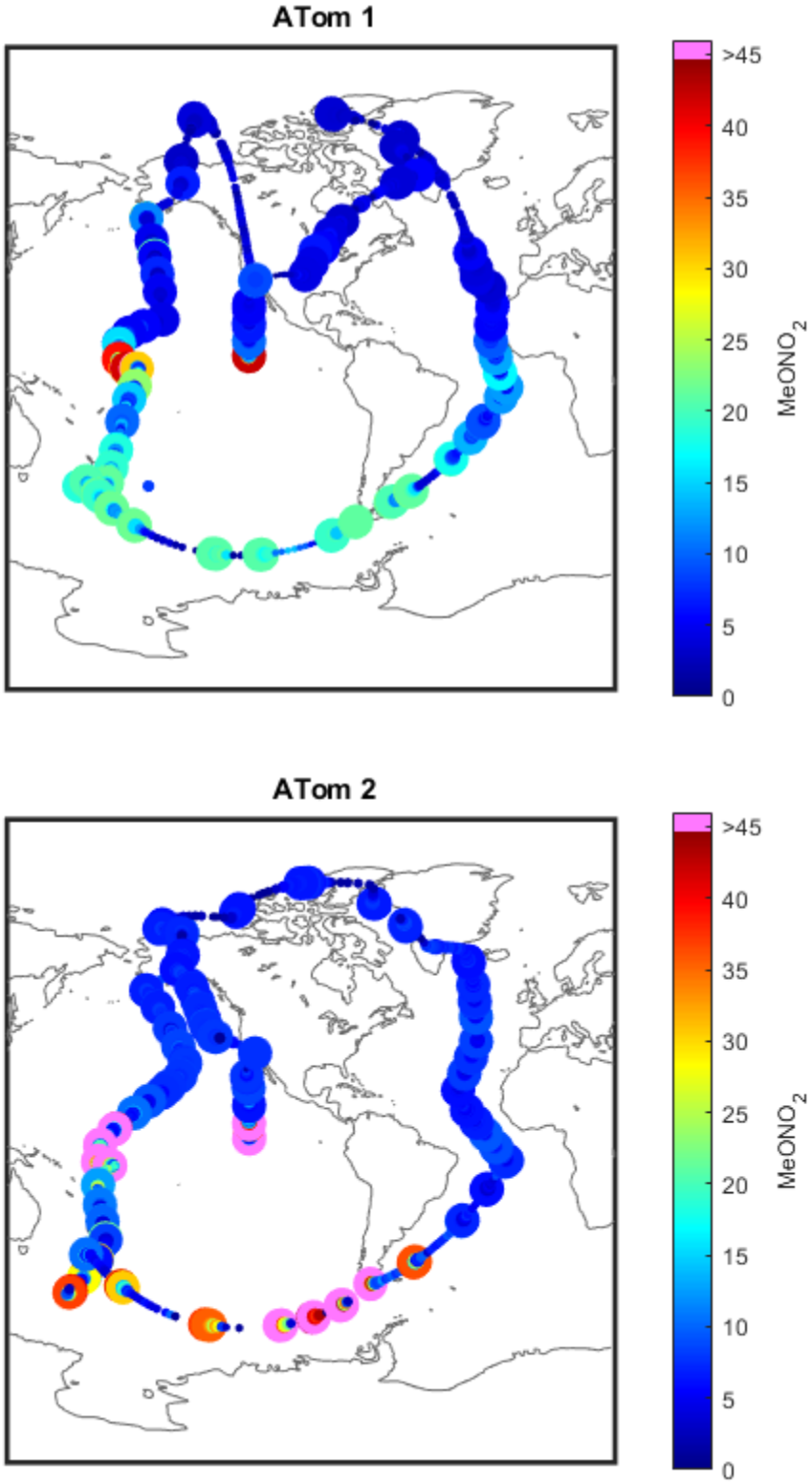

Figure 3.4 Methyl nitrate during ATom 1 (Jul-Aug, 2016) and ATom 2 (Jan-Feb, 2017). Larger size corresponds to lower altitude. Altitude range from ~ 500 – 40000 ft.

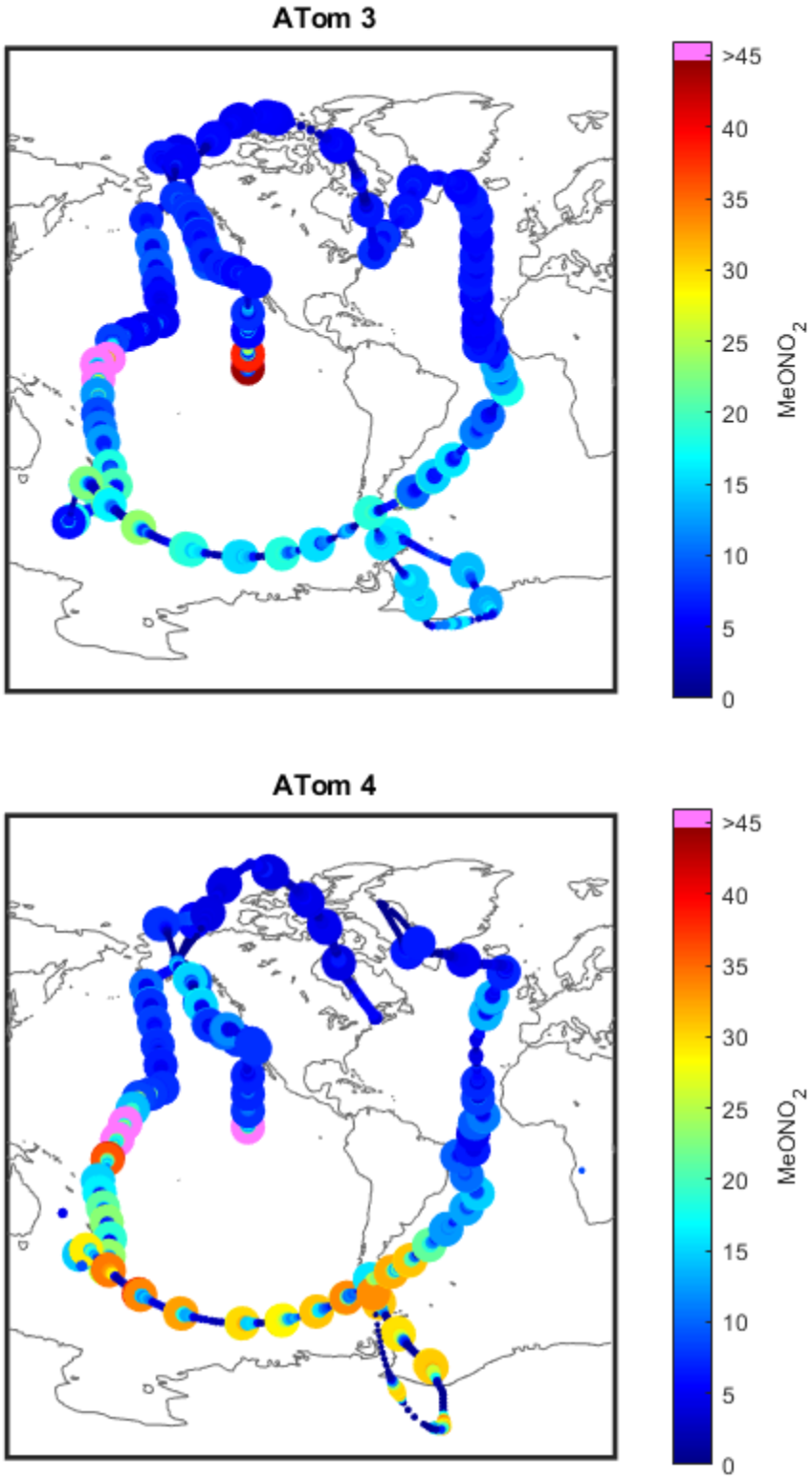

Figure 3.5 Methyl nitrate during ATom 3 (Sept-Oct, 2017) and ATom 4 (Apr-May, 2018). Larger size corresponds to lower altitude. Altitude range from ~ 500 – 40000 ft.

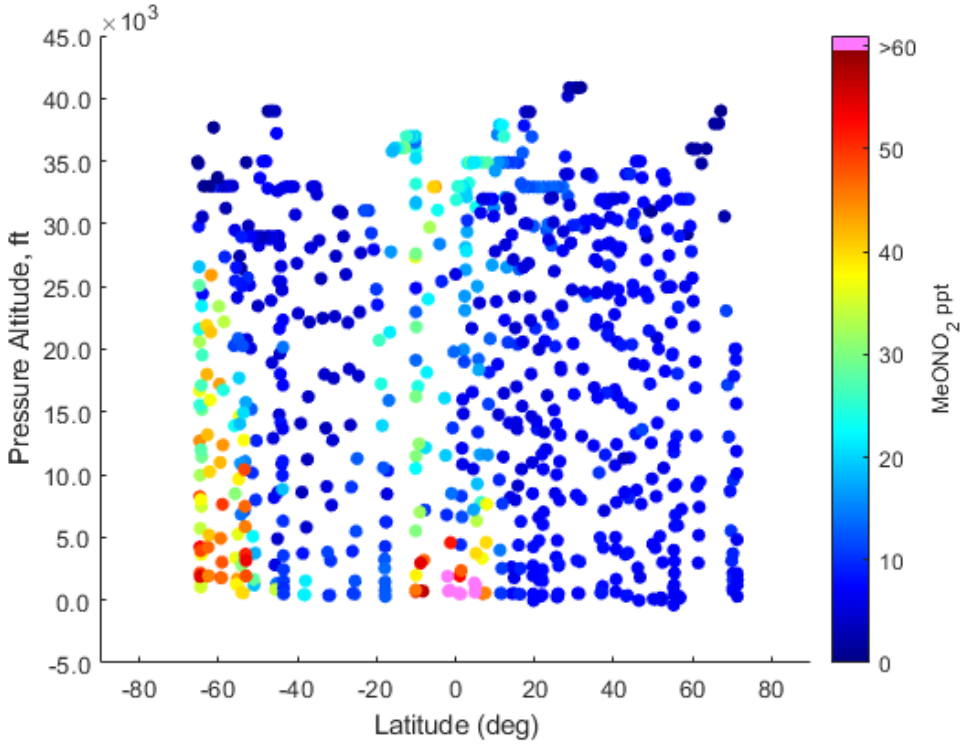

Figure 3.6 Flight transects across the equatorial Pacific during ATom 2 (Flights 1- 6), colored by $MeONO_2$ mixing ratio.

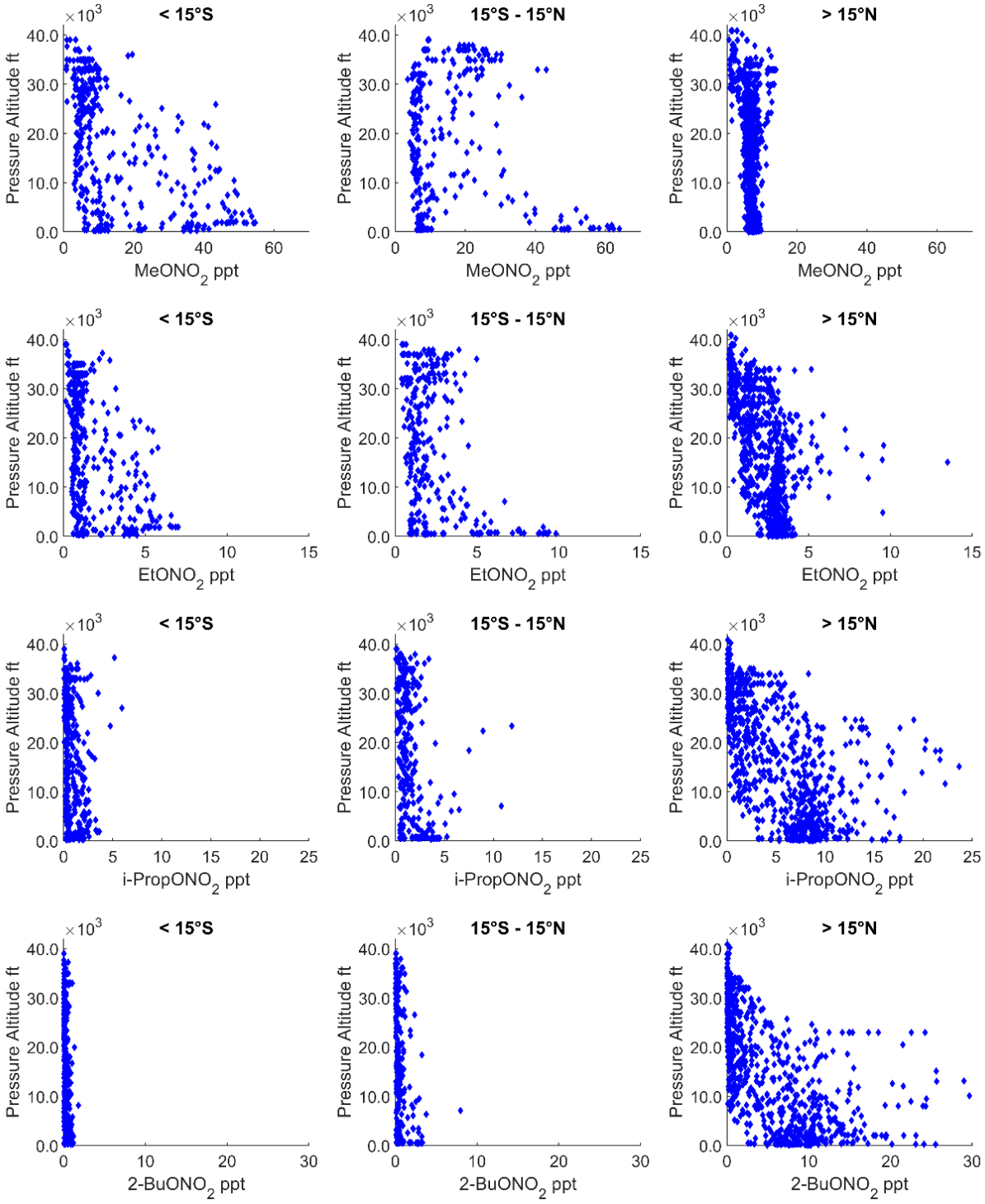

Figure 3.7 Vertical profiles of C_1-C_4 Alkyl Nitrates during ATom 2.

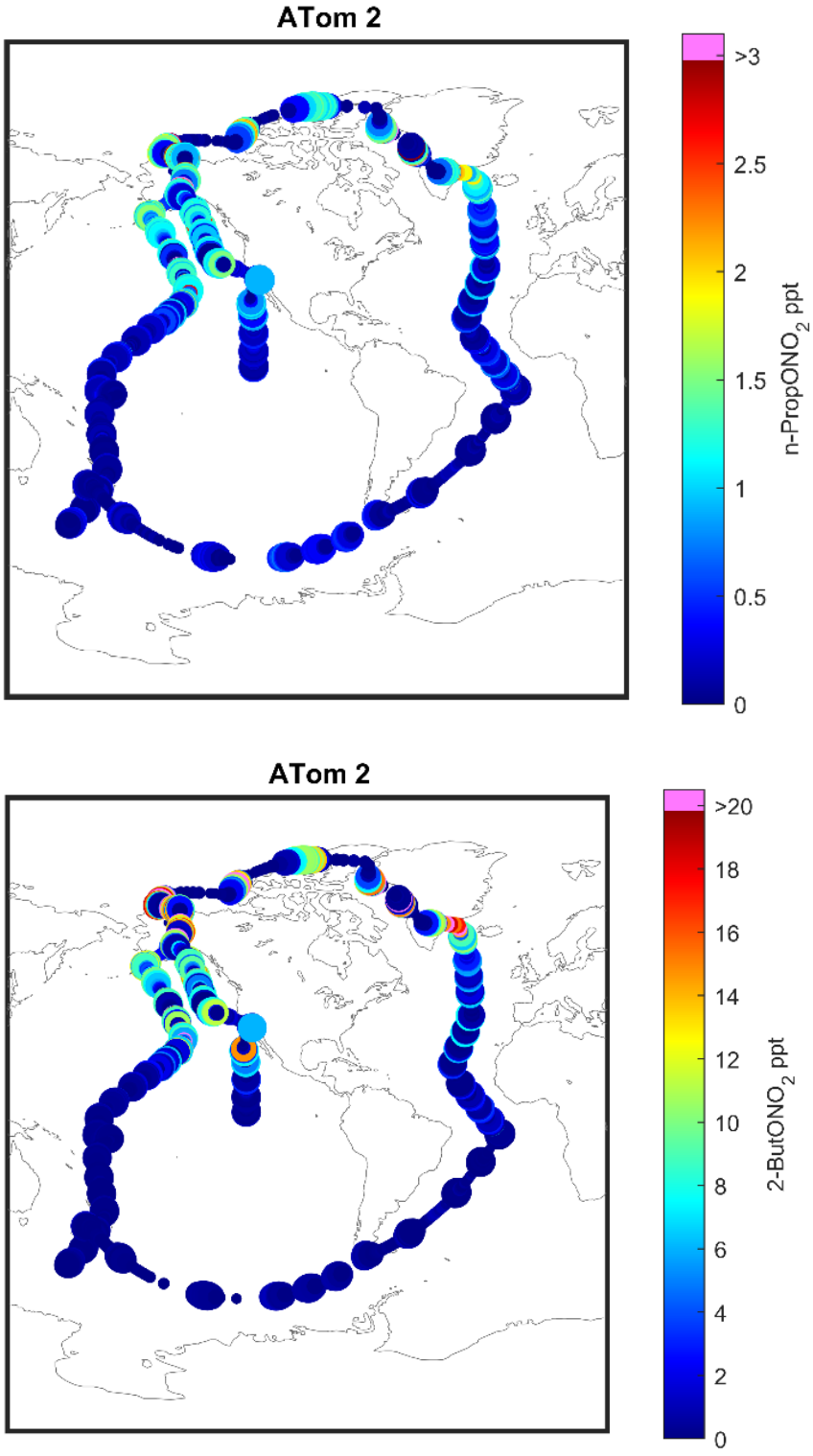

Figure 3.8 C_3-C_4 Alkyl Nitrates during ATom 2, larger markers indicate lower altitude. Altitude range from ~ 500 – 40000 ft.

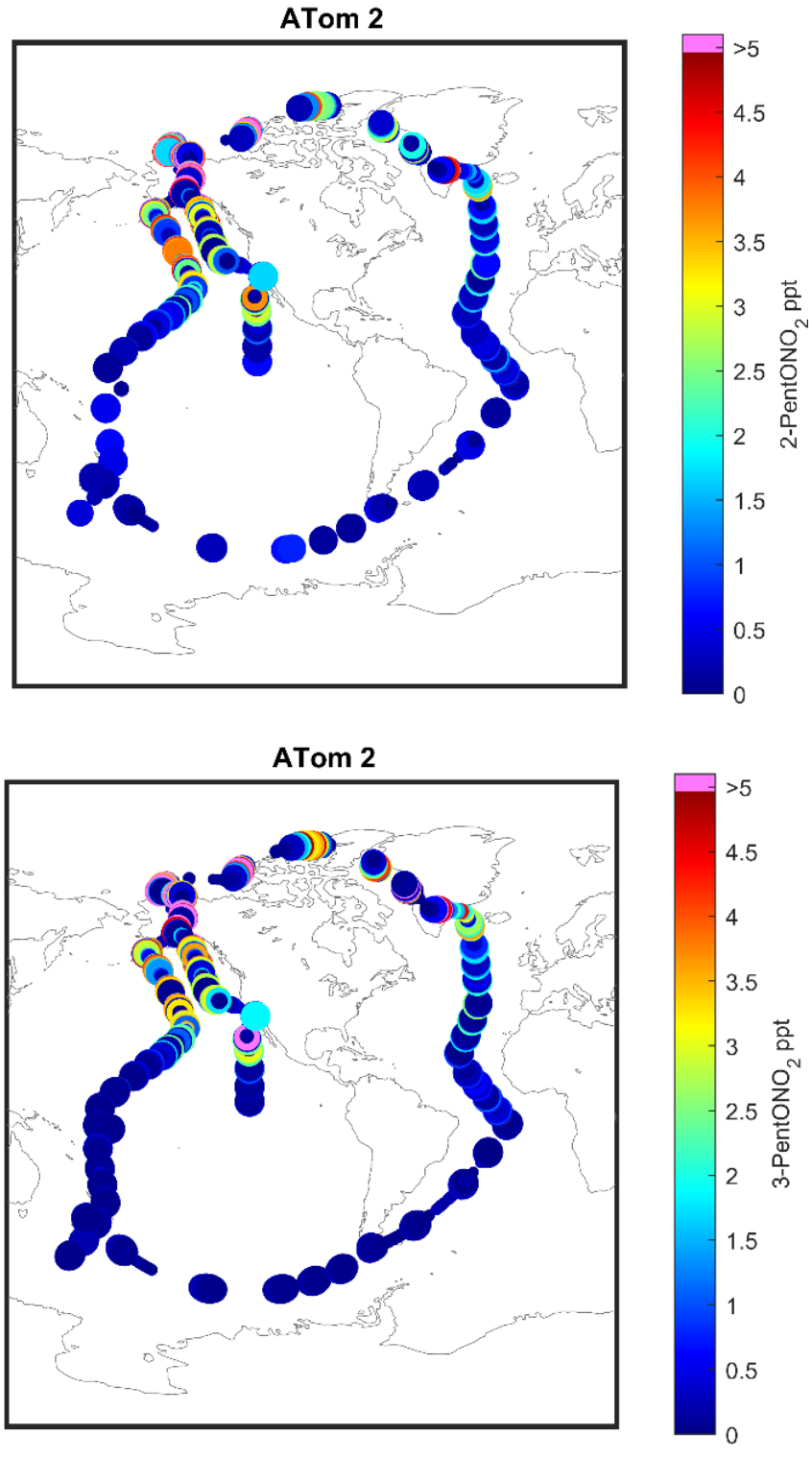

Figure 3.9 C_5 Alkyl nitrates during ATom 2, larger markers indicate lower altitude. Altitude range from ~ 500 – 40000 ft.

3.2.1 Sources of C_1- C_4 Alkyl Nitrates

While the ocean emissions provided the primary source of light alkyl nitrates across the globe, sufficiently polluted continental air accounted for a substantial portion of alkyl nitrate emissions. Figure 3.10 compares mixing ratios of $MeONO_2$ with urban and oceanic source tracers at all latitudes during the Northern Hemisphere winter. Tetrachloroethene (C_2Cl_4), a dry solvent with entirely anthropogenic production, is a useful tracer for industrial activity (Simpson et al., 2004). With an atmospheric lifetime of 3.5-4 months, C_2Cl_4 can undergo long range transport. Comparing $MeONO_2$ to C_2Cl_4, measurements taken during ATom 2 at >15°N have no significant correlation. When compared to $CHBr_3$, a biogenic ocean tracer (Atlas et al., 1993), $MeONO_2$ has some correlation ($R^2 = 0.32$) in the boundary layer of tropics and Southern Ocean, although there are confounding latitudinal effects to the fit.

EtONO2 follows many of the same trends as $MeONO_2$ in the tropics/ southern hemisphere, albeit with a greater contribution from photochemical sources (Figure 3.11). When compared to C_2Cl_4, EtONO2 has a stronger correlation ($R^2 = 0.58$) which indicates the more prominent photochemical source relative to $MeONO_2$ in the northern latitudes (>15°N).

The C_3-C_4 alkyl nitrates mark a shift in source trends for monofunctional alkyl nitrates, with the major source being photochemical production in northern hemisphere (Figure 3.12-13). While it is suspected that the oceans still provide a significant source, i-propyl nitrate is less correlated with oceanic tracers than the lighter nitrates, with an R^2 of 0.15 when compared to $MeONO_2$ in the tropics and southern hemisphere. C_4 nitrates have also been speculated to have a limited oceanic source (Blake et al., 2003), yet they have been excluded from recent modeling studies of oceanic alkyl nitrate emissions. Figure 3.14 shows the correlation between 2-$BuONO_2$ and $MeONO_2$, with the least squares fit excluding data from >15° S, to filter out continental influence. In the tropics, as well as the Southern Ocean, 2-$BuONO_2$ exhibits a significant correlation ($R^2 = 0.48$) with $MeONO_2$ which suggests that there is indeed be ocean flux of longer straight chain alkyl nitrates.

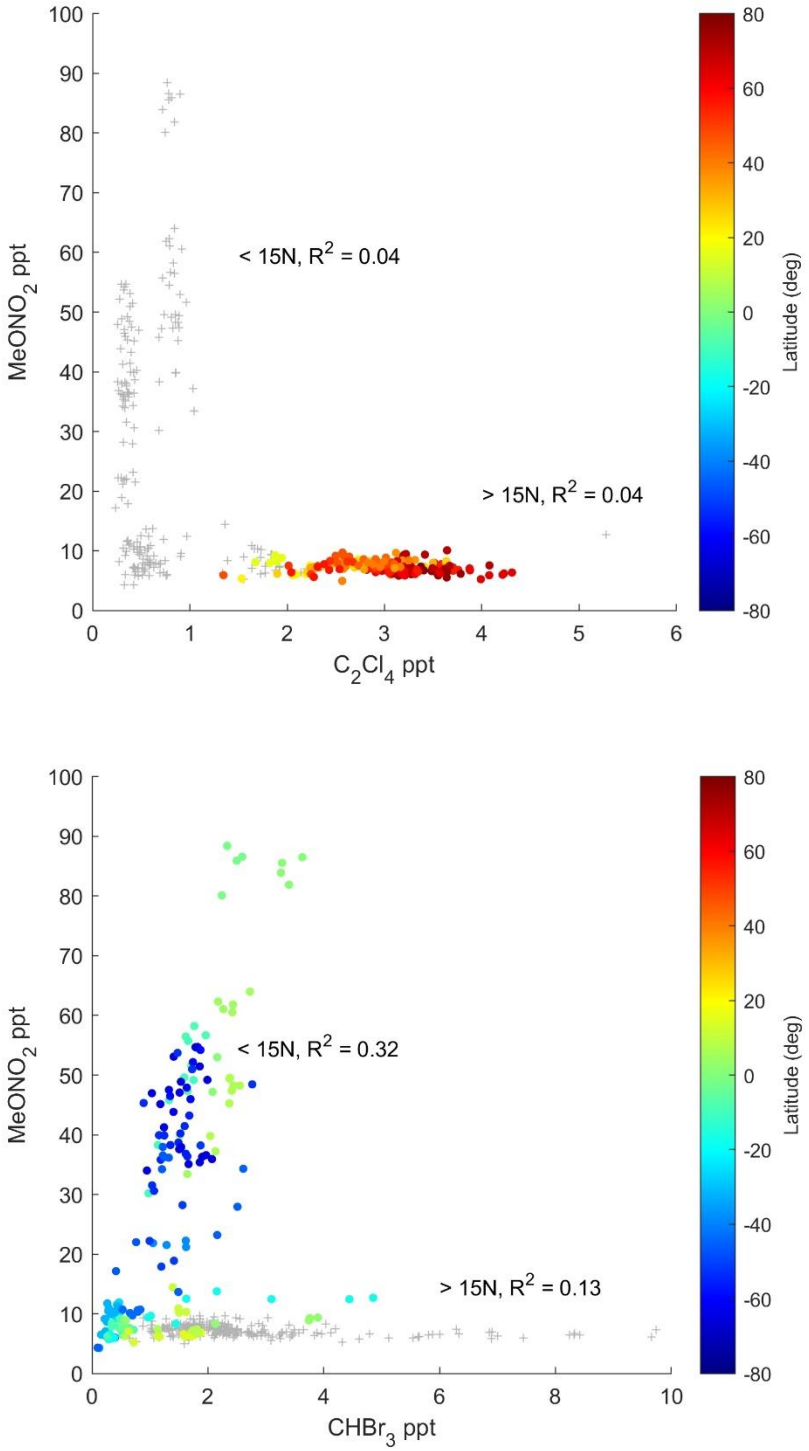

Figure 3.10 Correlations of $MeONO_2$ in the boundary layer (0-2 km) with anthropogenic and ocean tracers during ATom 2. For correlation with $CHBr_3$, (N=659)

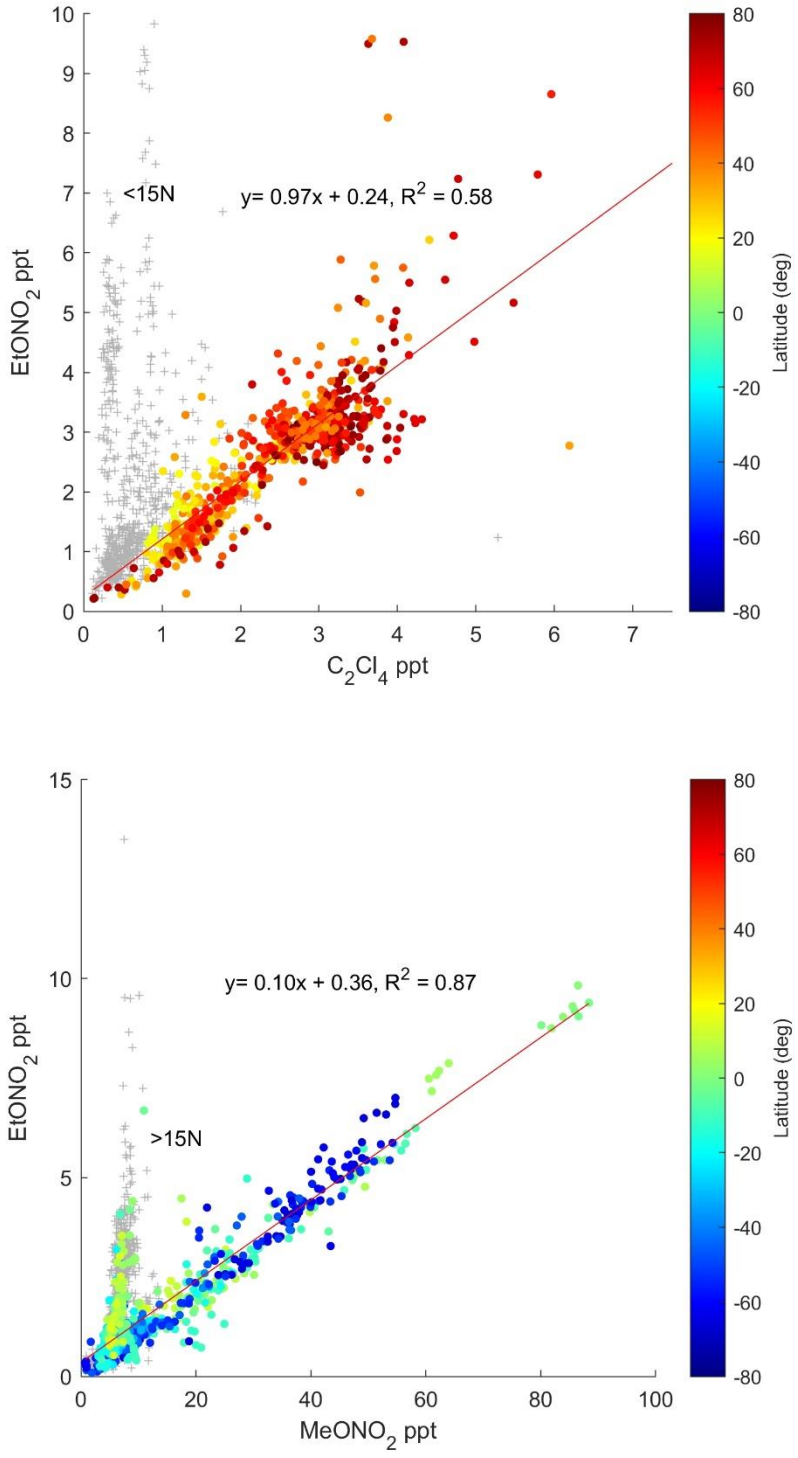

Figure 3.11 Correlation diagrams of $EtONO_2$ in the boundary layer (0-2 km) during ATom 2 with anthropogenic and ocean tracers. (N = 701, 692 respectively)

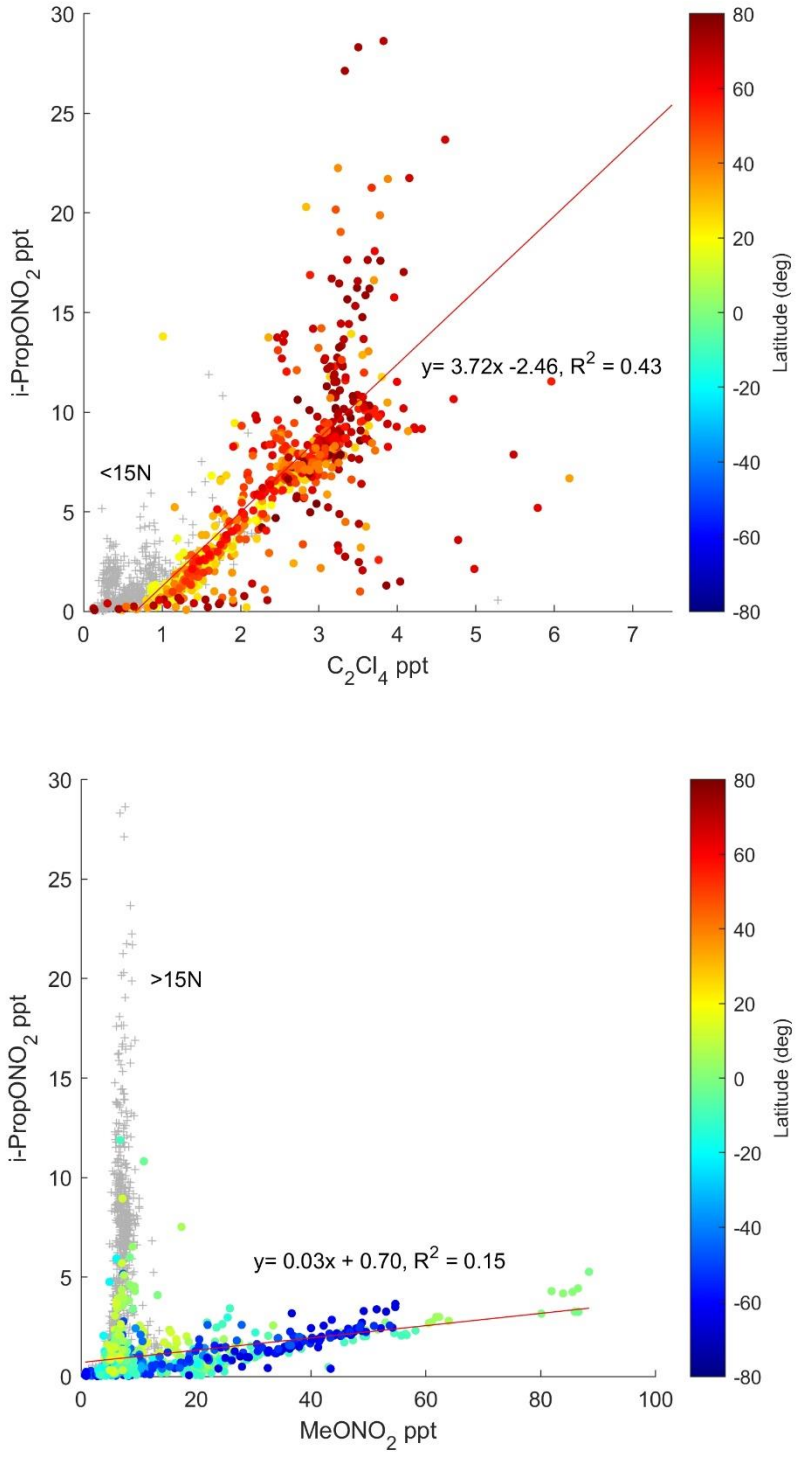

Figure 3.12 Correlation diagrams of i-propyl nitrate in the boundary layer (0-2 km) during ATom 2 with anthropogenic and ocean tracers. (N = 701, 692 respectively)

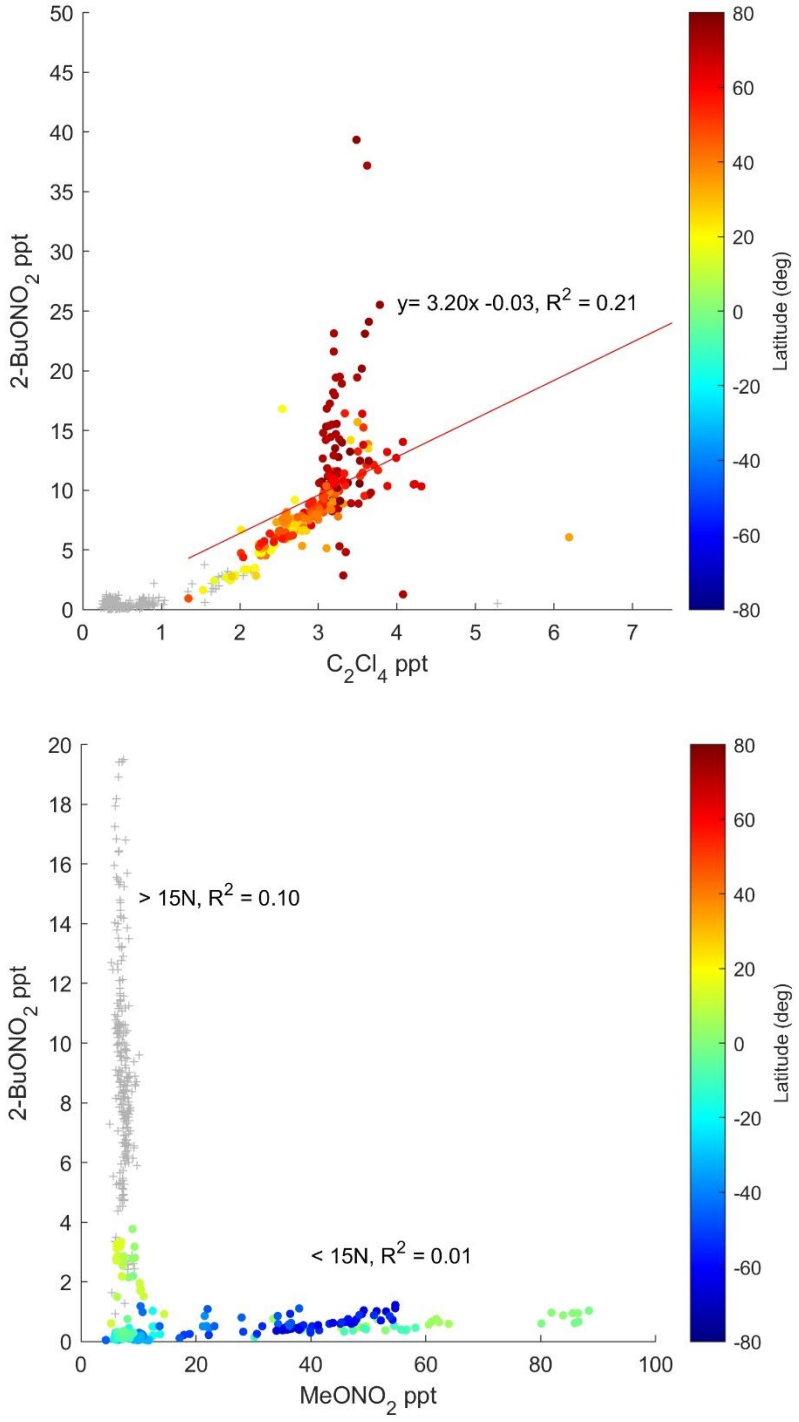

Figure 3.13 Correlation diagrams of 2-butyl nitrate in the boundary layer (0-2 km) during ATom 2 with anthropogenic and ocean tracers. (N = 701, 670 respectively)

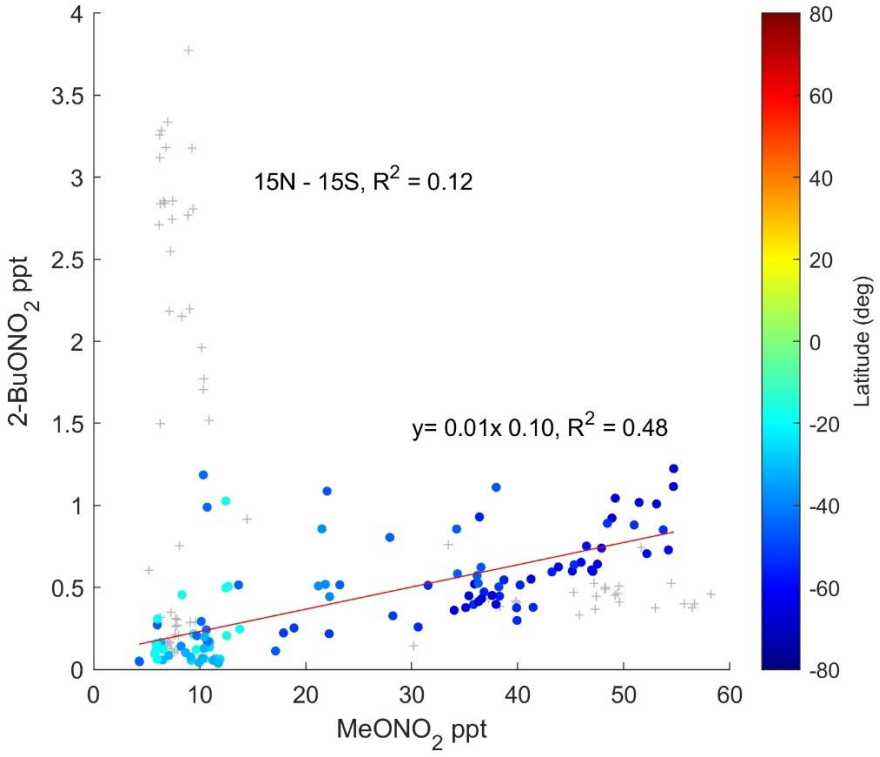

Figure 3.14 Correlation diagram of 2-$BuONO_2$ in the boundary layer south of the tropics (< 15° S) during ATom 2 to highlight ocean source. (N= 104).

3.2.2 Seasonal Trends

While regional maxima were spatially consistent, the magnitude of these maxima showed substantial temporal variations. Table 3.2 summarizes the seasonal data of C_1-C_4 alkyl nitrates observed in boundary layer for all of ATom. The highest mixing ratios of C_1-C_2 alkyl nitrates were observed during the Austral summer, which coincides with increased regional net primary production in the Southern surface ocean (Lutz et al., 2007). However, seasonal variations in the equatorial oceans (Figure 3.15), where oceanic biological production is near-constant, are more difficult to explain. Chuck et al.(2002) observed methyl/ethyl supersaturation events of up to 800% in the equatorial Atlantic during two separate cruises, conducted one year apart. Both cruises took place between September and October when observed ATom values for methyl/ethyl nitrate were not at their maximum. It is possible that

more of the precursors of light alkyl nitrates are available during the Austral winter. Given the aforementioned supersaturation events, it is also possible that seasonal ocean dynamics allow more favorable conditions for gas exchange from the surface ocean to the atmosphere, 'unloading' the supersaturated surface water and contributing to the equatorial maxima seen in Figure 3.16, from Jan-Feb (Carpenter et al., 2012).

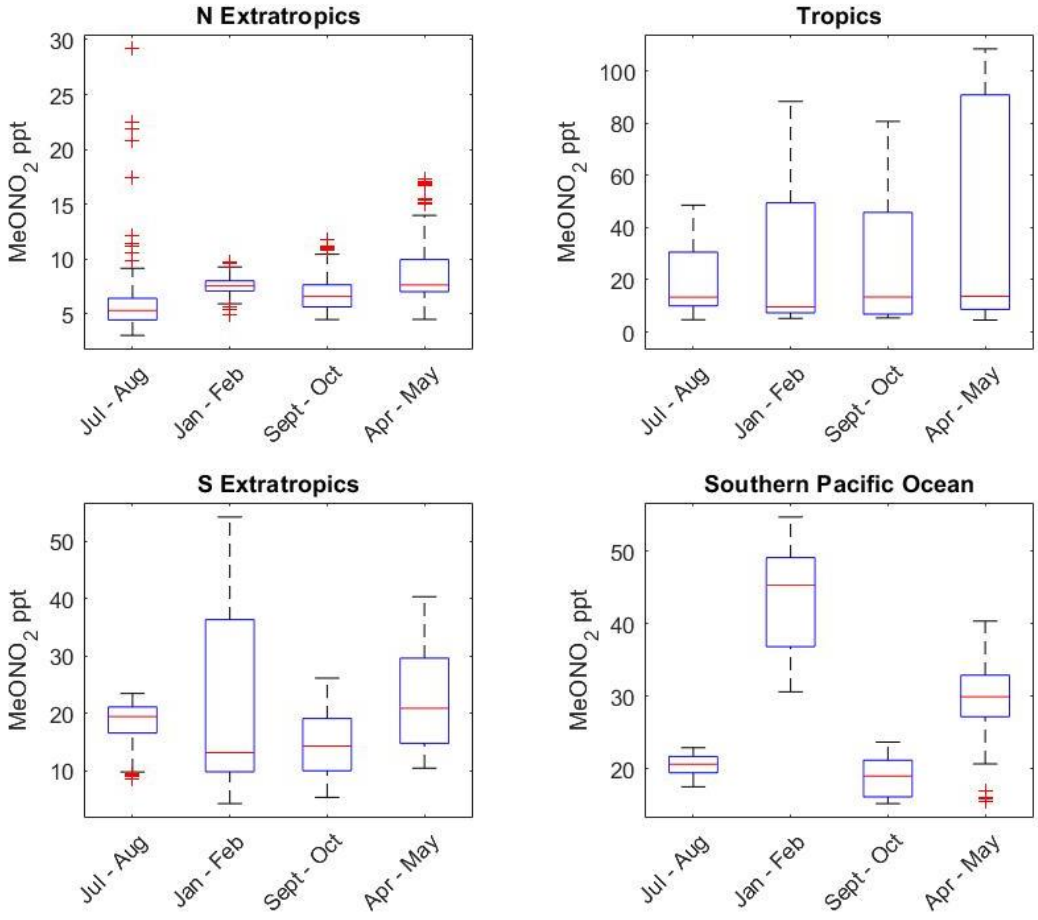

Figure 3.15 Box plots of $MeONO_2$ mixing ratios measured in the boundary layer (0-2km). Each index corresponds to an Atom deployment. The Southern Pacific Ocean tile denotes data from flights between Christchurch, NZ to Punta Arenas, Chile.

Table 3.2 Summary of ATom C_1-C_4 $RONO_2$ mixing ratios in the boundary layer (0-2km). All values are in ppt.

	MeONO2				EtONO2				i-PropONO2				2-BuONO2			
ATOM	1	**2**	3	**4**	1	**2**	3	**4**	1	**2**	3	**4**	1	**2**	3	**4**
N =(216, 243, 283, 234)	*Latitudes > 15° N*															
Min	2.4	**5.0**	4.5	**3.7**	0.8	**1.2**	0.8	**1.1**	0.5	**1.6**	0.5	**1.0**	0.1	**0.9**	0.1	**0.3**
Max	29.2	**10.1**	11.8	**17.3**	7.2	**9.5**	3.5	**6.2**	26.6	**31.2**	11.0	**19.0**	53.4	**39.3**	13.0	**18.9**
Median	4.8	**7.3**	6.2	**7.3**	1.5	**3.0**	1.8	**2.6**	1.8	**7.8**	3.0	**3.9**	1.0	**8.8**	2.6	**2.0**
Mean	5.4	**7.3**	6.5	**7.7**	1.9	**3.0**	1.8	**2.7**	3.3	**8.3**	3.0	**4.1**	3.8	**9.7**	2.5	**2.6**
SD	2.9	**0.9**	1.3	**2.9**	1.1	**0.6**	0.4	**0.8**	3.9	**2.9**	1.3	**2.0**	6.9	**4.9**	1.6	**2.0**
N =(86, 85, 68, 74)	*Latitudes 15° N -15° S*															
Min	4.7	**5.2**	5.4	**4.5**	0.9	**0.9**	0.7	**0.6**	0.3	**0.4**	0.4	**0.2**	0.1	**0.1**	0.1	**0.1**
Max	48.7	**88.4**	80.8	**108.6**	7.6	**9.8**	7.2	**10.6**	3.4	**6.5**	3.0	**4.6**	1.9	**3.8**	2.0	**2.3**
Median	13.4	**9.6**	13.4	**13.7**	2.8	**2.9**	1.8	**2.6**	1.7	**2.3**	1.6	**2.0**	0.7	**0.5**	0.4	**0.6**
Mean	20.6	**29.4**	26.1	**40.6**	3.3	**3.7**	2.8	**4.4**	1.7	**2.4**	1.6	**2.0**	0.7	**1.1**	0.6	**0.5**
SD	13.9	**27.0**	23.1	**38.7**	2.0	**2.6**	1.9	**3.6**	0.8	**1.4**	0.7	**1.1**	0.4	**1.1**	0.5	**0.4**
N =(131, 104, 121, 122)	*Latitudes < 15° S*															
Min	8.5	**4.3**	5.4	**10.5**	1.0	**0.5**	0.7	**1.1**	0.4	**0.1**	0.3	**0.3**	0.1	**0.0**	0.0	**0.1**
Max	23.5	**54.7**	26.2	**40.4**	5.2	**7.0**	3.6	**4.0**	4.4	**3.7**	3.0	**2.0**	2.8	**1.2**	3.4	**1.3**
Median	19.6	**22.2**	15.6	**21.8**	3.7	**2.7**	1.9	**2.3**	1.6	**1.4**	0.8	**1.0**	0.8	**0.4**	0.3	**0.4**
Mean	18.4	**26.0**	15.1	**22.4**	3.4	**2.9**	1.8	**2.4**	1.6	**1.3**	0.9	**1.0**	0.9	**0.4**	0.4	**0.4**
SD	3.9	**16.4**	5.0	**7.7**	0.9	**1.9**	0.7	**1.0**	0.5	**0.9**	0.5	**0.4**	0.3	**0.3**	0.6	**0.2**

For the longer, more anthropogenic sourced alkyl nitrates, maxima were observed in the Northern Hemisphere winter (Figure 3.17), where the reduced insolation leads to a decrease in photolysis, the primary fate for C_1-C_5 alkyl nitrates. However, this also causes reduced photochemical production of the C_2-C_5 alkyl nitrates. The increased effective lifetimes of these species allow them to undergo relatively longer transport, allowing advection from areas of increased photochemistry to areas of reduced insolation, where these species can concentrate.

For the oceanic species, it is important to note that the ATom mission took place during two El Niño Southern Oscillation (ENSO) events: El Niño for ATom 1, neutral for ATom 2 and La Niña for ATom 3-4 (Dewitt, 2020). El Niño events are marked by warmer sea surface temperature as well as stronger upwelling and convection in the tropics (Oort and Yienger, 1996). It is poorly understood how these phenomena, and their evolution through climate change, will impact the lifecycle of alkyl nitrates (Fisher et al., 2018). As ENSO introduces interannual variability, it will be important future work to quantify the impacts of ENSO on alkyl nitrate emissions.

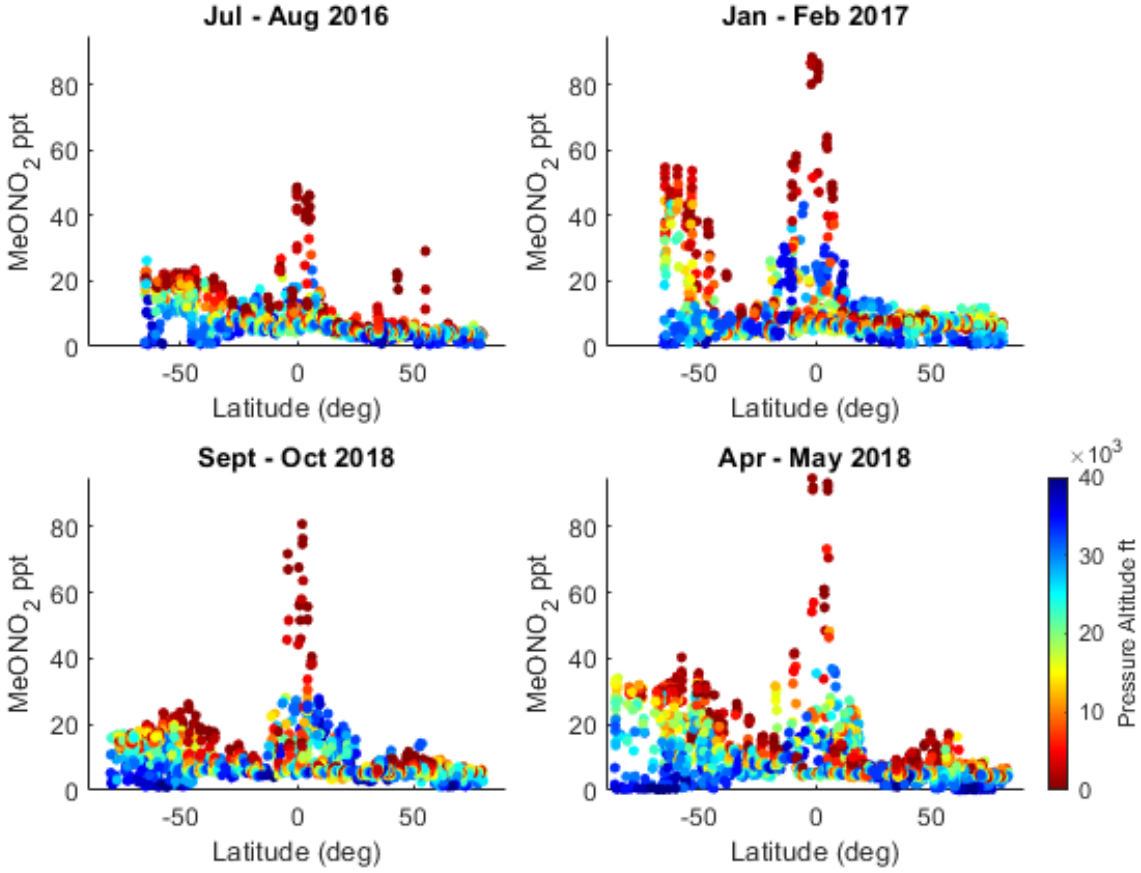

Figure 3.16 Global latitudinal distribution of $MeONO_2$ by season.

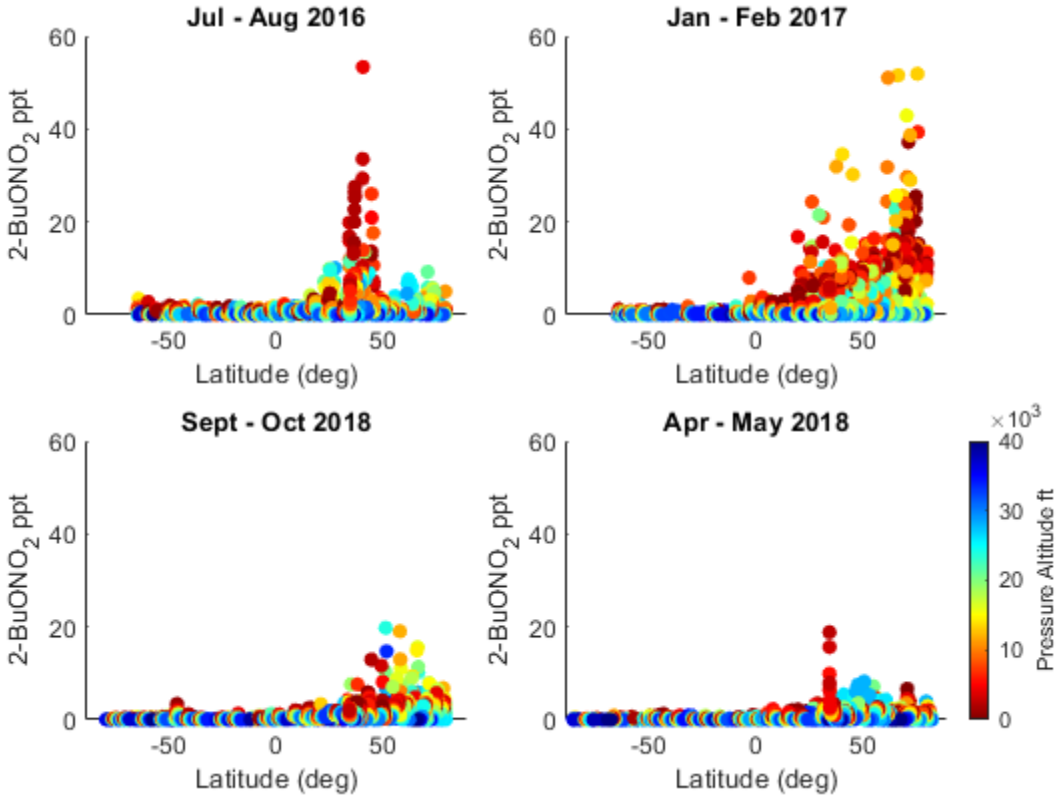

Figure 3.17 Global latitudinal distribution of 2-$BuONO_2$ by season.

3.2.3 Pacific and Atlantic Ocean Inter-comparison

Perhaps more striking than the seasonal fluctuation in the oceanic alkyl nitrates is the stark difference in overall observed mixing ratios between the Pacific and Atlantic Oceans. Figure 3.18 shows mixing ratios of methyl nitrate in the equatorial Pacific were consistently higher (up to a factor of 9) than in the Atlantic, as well as midlatitudes, contributing to a sizable longitudinal gradient. Only the southern-most sampled area of the Atlantic exhibited mixing ratios that were somewhat consistent with observations of the central/south Pacific. Oceanic alkyl nitrate formation is dependent upon the alkyl peroxy radicals created by the photolysis of colored dissolved organic matter (CDOM) (Dahl et al., 2003; 2007). It is conceivable that the controls on CDOM distribution would have similar effects on alkyl nitrate generation. However, satellite and in-situ data show only small, regional differences in surface CDOM concentrations between the Pacific and Atlantic oceans (Nelson and Siegel, 2013). This suggests that CDOM

quantity alone is not a good indication of alkyl nitrate production. Nitrate ion in the surface ocean has also been shown to exert controls on CDOM photoreactivity (Swan et al., 2012), although changes in the photoreactivity were not dependent on the quantity, but the chemical composition of the CDOM being irradiated. It is possible that CDOM composition has a significant impact on the potential for alkyl nitrate production. However, the complexity of CDOM as a mixture makes it very difficult to characterize, which presents challenges in trying to locate the exact conditions that promote generation of alkyl nitrates.

In addition to CDOM, alkyl nitrate production is also dependent upon the photolysis products of nitrite (Dahl et al., 2003). Ocean nitrite is a major intermediate the nitrification/denitrification processes and has important links to oceanic primary production (Martin et al., 2019; Bristow et al., 2017). With the apparent availability of CDOM in both the Atlantic and Pacific (Figure 3.19), it is feasible that the production of oceanic alkyl nitrates is primarily limited by available nitrite. Thus, the longitudinal gradient of ocean alkyl nitrates may be explained by differences in nutrient cycling, in addition to differences in wind speeds and ocean circulation.

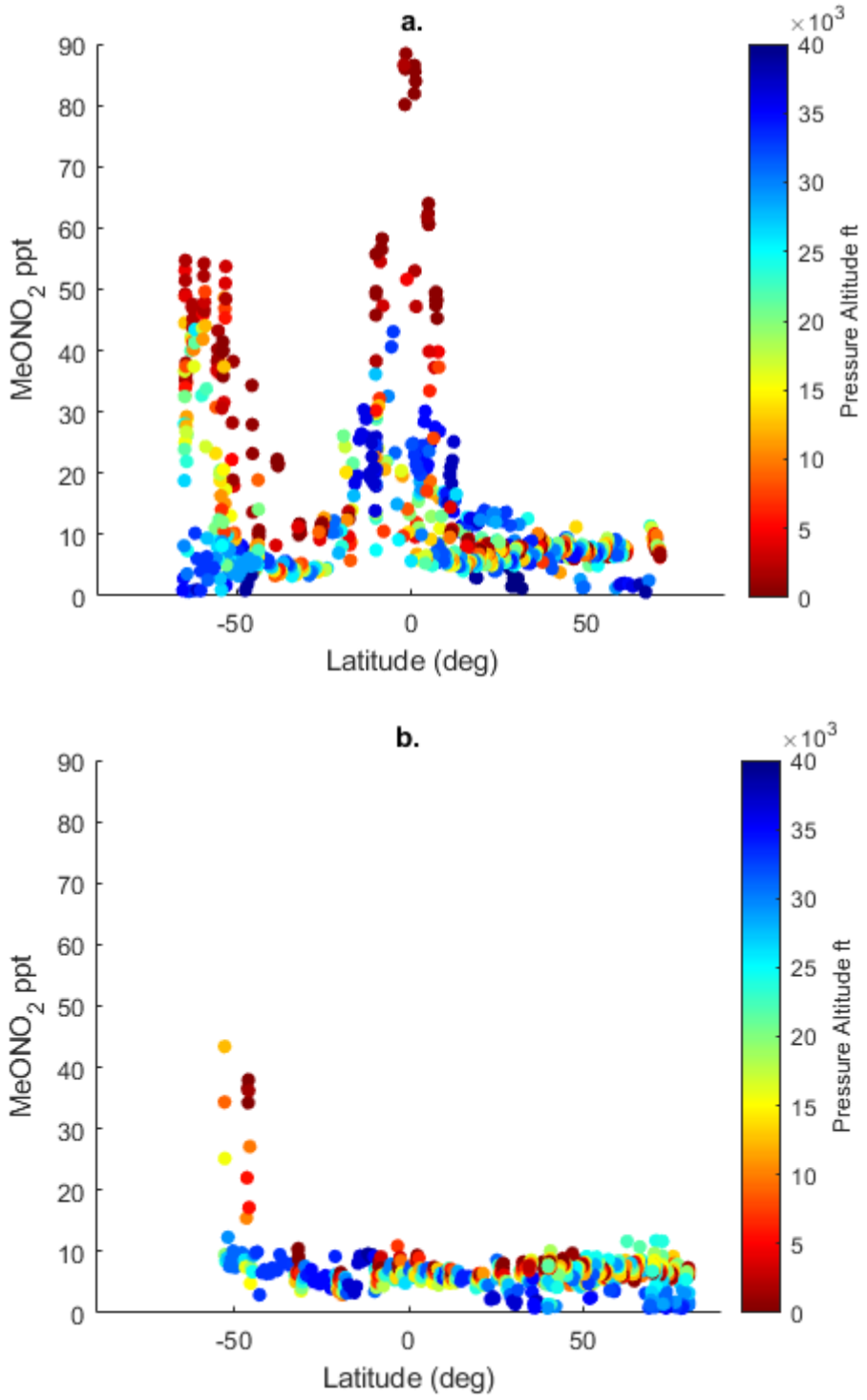

Figure 3.18 Latitudinal distribution of $MeONO_2$ in the Pacific (a) and Atlantic (b) Oceans during ATom 2

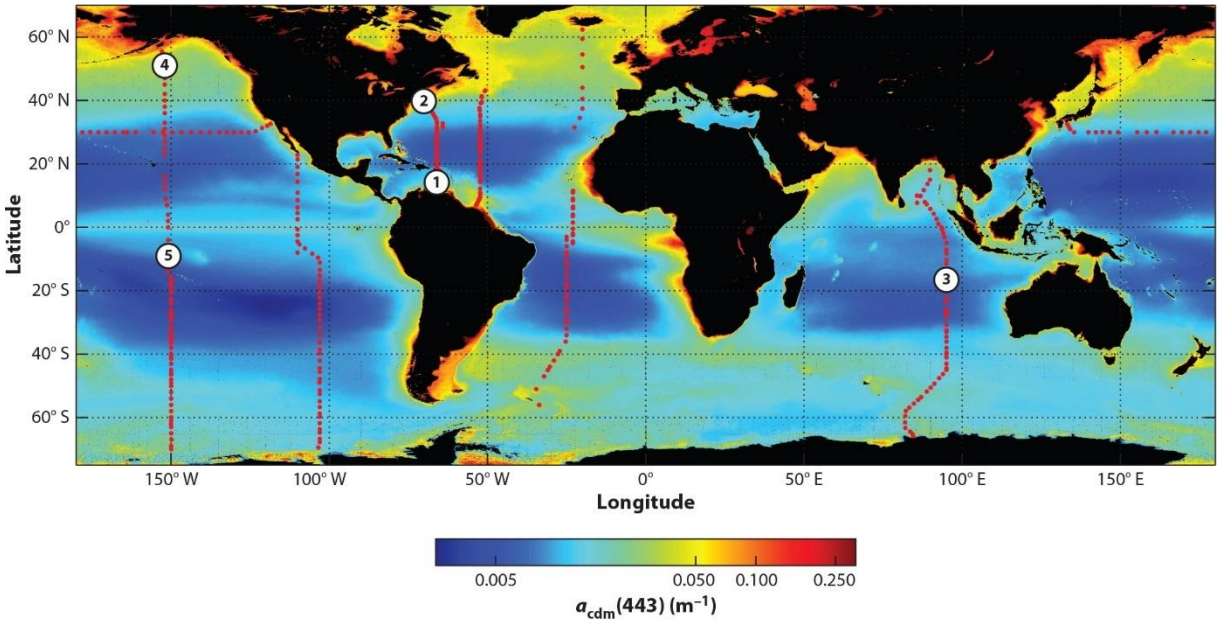

Figure 3.19 Global surface ocean distribution of CDOM plus detrital particle absorption (α_{CDOM} at 443mn) derived from the Garver-Siegel-Maritorena bio-optical model applied to ocean color data from SeaWiFS (Sea-Viewing Wide Field-of-View Sensor) satellite mission. Data shown are the 1997-2010 mean. Red circles denote surface in situ samples, higher absorption indicates higher CDOM concentration. Adapted from Nelson and Siegel(2013).

3.3 Ocean Alkyl Nitrates in the Tropical Stratosphere

Strong convection due to tropical upwelling is a driving force for both tropospheric and stratospheric circulation. This system, known as the Brewer-Dobson circulation, describes how air from the low tropical stratosphere is transported to higher latitudes, where it sinks and potentially reenters the troposphere (Avallone and Prather, 1996). This stratospheric outflow is fed by the strong convection in the tropics which is transported into the stratosphere through the Tropical Tropopause Layer (TTL) (Plumb and Eluszkiewicz, 1999).

While the effects of Brewer-Dobson circulation on long-lived tracers have been historically well considered (Hegglin et al., 2006), recent work has focused on the impacts of shorter-lived tracers. For example, many of the compounds known as very short-lived substances (VSLS) have oceanic sources and have the capacity to be ozone depleting substances. The 'tropical pipe' allows for these trace gas species to be transported from the surface to the stratosphere on timescales that coincide with their atmospheric lifetimes (Aschmann and

Sinnhuber, 2013). Levine et al (2007) demonstrates that a significant fraction of certain VSLS can make it to the stratosphere, where they can enact catalytic ozone destruction.

In contrast to the troposphere, NO_x participates in the destruction of stratospheric O_3 by interfering with its regeneration via the Chapman mechanism (Portmann et al., 2012). C_1-C_3 alkyl nitrates, as reservoirs of NO_x, have average atmospheric lifetimes on the order of some VSLS (26 days, 14 days and 8 days, from C_1 to C_3, respectively) (Fisher et al., 2018). In this regard, short-chained alkyl nitrates and VSLS exhibit some interesting similarities: they both have oceanic sources, potentially deplete ozone (in the stratosphere), are common within the tropics and have comparable lifetimes. To my knowledge, there has been no work that has investigated the possibility of ocean alkyl nitrates undergoing transport from the TTL to the stratosphere or their subsequent impact on stratospheric chemistry. Models of an ideal trace gas with a constant loss rate showed that 1.2% to 4.9% of surface emissions (for gases with lifetimes of 8 days and 21 days, respectively) of an 'ocean-like' source are transported to the stratosphere (Holzer and Polvani, 2013). For example, estimating 4.9% of surface emissions using the range of $MeONO_2$ mixing ratios measured in the tropical boundary layer during ATom 4, (Table 3.2), would mean an estimated ~0.22- 5.3 ppt of $MeONO_2$ entering the stratosphere. VSLS models that incorporate more sophisticated chemistry and dynamics show similar results with 0.5-1% and 3-4% for gases with 7 day and 28 day lifetimes (Levine et al., 2007). With ATom measurements of $MeONO_2$ alone exceeding 100 ppt in the tropics, the amount of odd nitrogen imported into the stratosphere may have significant impacts.

NO_y transport from the TTL into the stratosphere has been investigated in airborne campaigns (Murphy et al., 1993) as well as modeling studies (Avallone and Prather, 1996). In general, NO_y is treated as having an atmospheric lifetime in the stratosphere that is long enough to undergo transport via Brewer-Dobson circulation and descend into the midlatitude troposphere. However, this study, as well as the in-situ measurements, do not account for the composition of NO_y. It is feasible that the reduced lifetimes of constituents such as short chain

alkyl nitrates may alter the NO_y dynamics in the lower stratosphere. Having a better grasp on the inventory of NO_y could better improve our understanding of these dynamics. In addition, climate change also poses potential impacts. ENSO strengthens tropical upwelling, allowing for greater tracer transport. It is possible that this may either lead to unforeseen ozone destruction or increase in stratosphere to troposphere transport (STT) in the mid-latitudes (Randel and Jensen, 2013).

REFERENCES

1. Wofsy, S. C.; Prather, M. J.; Ryerson, T. B.; Newman, P., Atmospheric Tomography Mission (ATom) Executive Summary. 2015.

2. Blake, N. J.; Blake, D. R.; Swanson, A. L.; Atlas, E.; Flocke, F.; Rowland, F. S., Latitudinal, vertical, and seasonal variations of C-1-C-4 alkyl nitrates in the troposphere over the Pacific Ocean during PEM-Tropics A and B: Oceanic and continental sources. *J. Geophys. Res.-Atmos.* **2003,** *108* (D2).

3. Fisher, J. A.; Atlas, E. L.; Barletta, B.; Meinardi, S.; Blake, D. R.; Thompson, C. R.; Ryerson, T. B.; Peischl, J.; Tzompa-Sosa, Z. A.; Murray, L. T., Methyl, Ethyl, and Propyl Nitrates: Global Distribution and Impacts on Reactive Nitrogen in Remote Marine Environments. *J. Geophys. Res.-Atmos.* **2018,** *123* (21), 12429-12451.

4. Simpson, I. J.; Meinardi, S.; Blake, N. J.; Rowland, F. S.; Blake, D. R., Long-term decrease in the global atmospheric burden of tetrachloroethene (C2Cl4). *Geophys. Res. Lett.* **2004,** *31* (8).

5. Atlas, E.; Pollock, W.; Greenberg, J.; Heidt, L.; Thompson, A. M., ALKYL NITRATES, NONMETHANE HYDROCARBONS, AND HALOCARBON GASES OVER THE EQUATORIAL PACIFIC-OCEAN DURING SAGA-3. *J. Geophys. Res.-Atmos.* **1993,** *98* (D9), 16933-16947.

6. Lutz, M. J.; Caldeira, K.; Dunbar, R. B.; Behrenfeld, M. J., Seasonal rhythms of net primary production and particulate organic carbon flux to depth describe the efficiency of biological pump in the global ocean. *Journal of Geophysical Research: Oceans* **2007,** *112* (C10).

7. Chuck, A. L.; Turner, S. M.; Liss, P. S., Direct evidence for a marine source of C-1 and C-2 alkyl nitrates. *Science* **2002,** *297* (5584), 1151-1154.

8. Carpenter, L. J.; Archer, S. D.; Beale, R., Ocean-atmosphere trace gas exchange. *Chemical Society Reviews* **2012,** *41* (19), 6473-6506.

9. Dewitt, D., Cold & Warm Episodes by Season. Center, N. C. P., Ed. 2020.

10. Oort, A. H.; Yienger, J. J., Observed Interannual Variability in the Hadley Circulation and Its Connection to ENSO. *Journal of Climate* **1996,** *9* (11), 2751-2767.

11. Dahl, E. E.; Saltzman, E. S.; de Bruyn, W. J., The aqueous phase yield of alkyl nitrates from ROO+NO: Implications for photochemical production in seawater. *Geophys. Res. Lett.* **2003,** *30* (6).

12. Dahl, E. E.; Yvon-Lewis, S. A.; Saltzman, E. S., Alkyl nitrate (C-1-C-3) depth profiles in the tropical Pacific Ocean. *Journal of Geophysical Research-Oceans* **2007,** *112* (C1).

13. Nelson, N. B.; Siegel, D. A., The global distribution and dynamics of chromophoric dissolved organic matter. *Annual review of marine science* **2013,** *5*, 447-476.

14. Swan, C. M.; Nelson, N. B.; Siegel, D. A.; Kostadinov, T. S., The effect of surface irradiance on the absorption spectrum of chromophoric dissolved organic matter in the global ocean. *Deep Sea Research Part I: Oceanographic Research Papers* **2012,** *63*, 52-64.

15. Martin, T. S.; Primeau, F.; Casciotti, K. L., Modeling oceanic nitrate and nitrite concentrations and isotopes using a 3-D inverse N cycle model. *Biogeosciences* **2019,** *16* (2), 347-367.

16. Bristow, L. A.; Mohr, W.; Ahmerkamp, S.; Kuypers, M. M., Nutrients that limit growth in the ocean. *Current Biology* **2017,** *27* (11), R474-R478.

17. Avallone, L. M.; Prather, M. J., Photochemical evolution of ozone in the lower tropical stratosphere. *J. Geophys. Res.-Atmos.* **1996,** *101* (D1), 1457-1461.

18. Plumb, R. A.; Eluszkiewicz, J., The Brewer-Dobson circulation: Dynamics of the tropical upwelling. *Journal of the Atmospheric Sciences* **1999,** *56* (6), 868-890.

19. Hegglin, M. I.; Brunner, D.; Peter, T.; Hoor, P.; Fischer, H.; Staehelin, J.; Krebsbach, M.; Schiller, C.; Parchatka, U.; Weers, U., Measurements of NO, NOy, N2O, and O-3 during SPURT: implications for transport and chemistry in the lowermost stratosphere. *Atmospheric Chemistry and Physics* **2006,** *6*, 1331-1350.

20. Aschmann, J.; Sinnhuber, B. M., Contribution of very short-lived substances to stratospheric bromine loading: uncertainties and constraints. *Atmospheric Chemistry and Physics* **2013,** *13* (3), 1203-1219.

21. Levine, J. G.; Braesicke, P.; Harris, N. R. P.; Savage, N. H.; Pyle, J. A., Pathways and timescales for troposphere-to-stratosphere transport via the tropical tropopause layer and their relevance for very short lived substances. *J. Geophys. Res.-Atmos.* **2007,** *112* (D4), 15.

22. Portmann, R.; Daniel, J.; Ravishankara, A., Stratospheric ozone depletion due to nitrous oxide: influences of other gases. *Philosophical Transactions of the Royal Society B: Biological Sciences* **2012,** *367* (1593), 1256-1264.

23. Holzer, M.; Polvani, L. M., Lifetime dependent flux into the lowermost stratosphere for idealized trace gases of surface origin. *J. Geophys. Res.-Atmos.* **2013,** *118* (16), 9367-9375.

24. Murphy, D. M.; Fahey, D. W.; Proffitt, M. H.; Liu, S. C.; Chan, K. R.; Eubank, C. S.; Kawa, S. R.; Kelly, K. K., Reactive nitrogen and its correlation with ozone in the lower stratosphere and upper troposphere. *Journal of Geophysical Research: Atmospheres* **1993,** *98* (D5), 8751-8773.

25. Randel, W. J.; Jensen, E. J., Physical processes in the tropical tropopause layer and their roles in a changing climate. *Nature Geoscience* **2013,** *6* (3), 169-176.

CHAPTER 4

Dimethyl Sulfide During ATom: Seasonal Fluctuations and Potential Impacts

Dimethyl sulfide (DMS) as a biogenic gas can have significant impacts on climate forcing by creating positive (and to a minor extent, negative) feedbacks with secondary products. DMS can exert controls on local radiative forcing by forming aerosol, causing backscatter of solar radiation. DMS can also form a subset of aerosol known as cloud condensation nuclei (CCN). In the remote atmosphere, especially near the poles, these CCNs can be sparse (Veres et al., 2020). As such, new particle formation due to DMS oxidation has powerful implications for cloud seeding, albedo and climate (Gali et al., 2019).

4.1 Global Distribution of DMS during ATom

As stated previously, DMS is emitted as a product of marine biotic activity. During ATom, DMS was observed primarily in the marine boundary layer, with enhancements in areas favoring increased marine primary production (i.e. tropical upwelling). However, these enhancements did not adhere to a latitudinal or longitudinal gradient. Figure 4.1 shows DMS measurements taken during ATom 2, in the Austral summer. DMS mixing ratios are elevated in the tropical Pacific and Southern Oceans, yet levels in the Atlantic were generally lower. This contrasts with the other deployments (Figure 4.2 - 4.3), in which the Atlantic shows some of the highest mixing ratios observed during the campaign. These elevated levels coincide with springtime plankton blooms in the North Atlantic (Sverdrup, 1953). This is likely due to the high variability of DMS precursor production by species of plankton, which can range 5 orders of magnitude (Andreae and Crutzen, 1997). Thus, the production of DMS, even in area of high primary production, is heavily contingent upon a gamut of factors (e.g., plankton population, ocean chemistry, etc.) (Gaston et al., 2011).

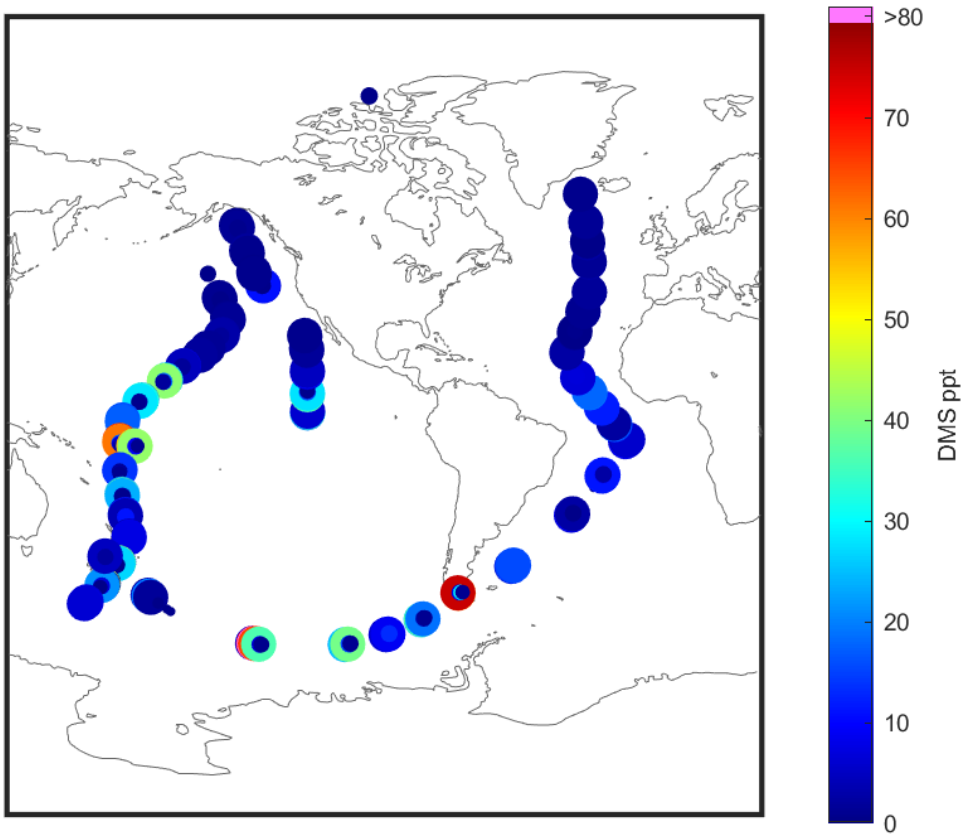

Figure 4.1 DMS during ATom 2, larger markers indicate lower altitude. Sample points below level of detection are omitted from flight transect. Altitude range from ~ 500 – 40000 ft.

This variability is evident across the measurements made during ATom. The tropics exhibit large DMS enhancements, due to nutrient availability in the tropical oceanic upwelling. Tropical convection is highlighted in the vertical profiles of Figure 4.4, where DMS enhancements are preserved in rapid transport to the free troposphere, despite its atmospheric lifetime of ~1 day (Meinardi et al., 2003). While the Pacific showed more consistent enhancements, regions in the Atlantic showed mixing ratios exceeding 100 ppt. Enhancements were also observed in the Southern Pacific during the austral summer, coinciding with increased biological production.

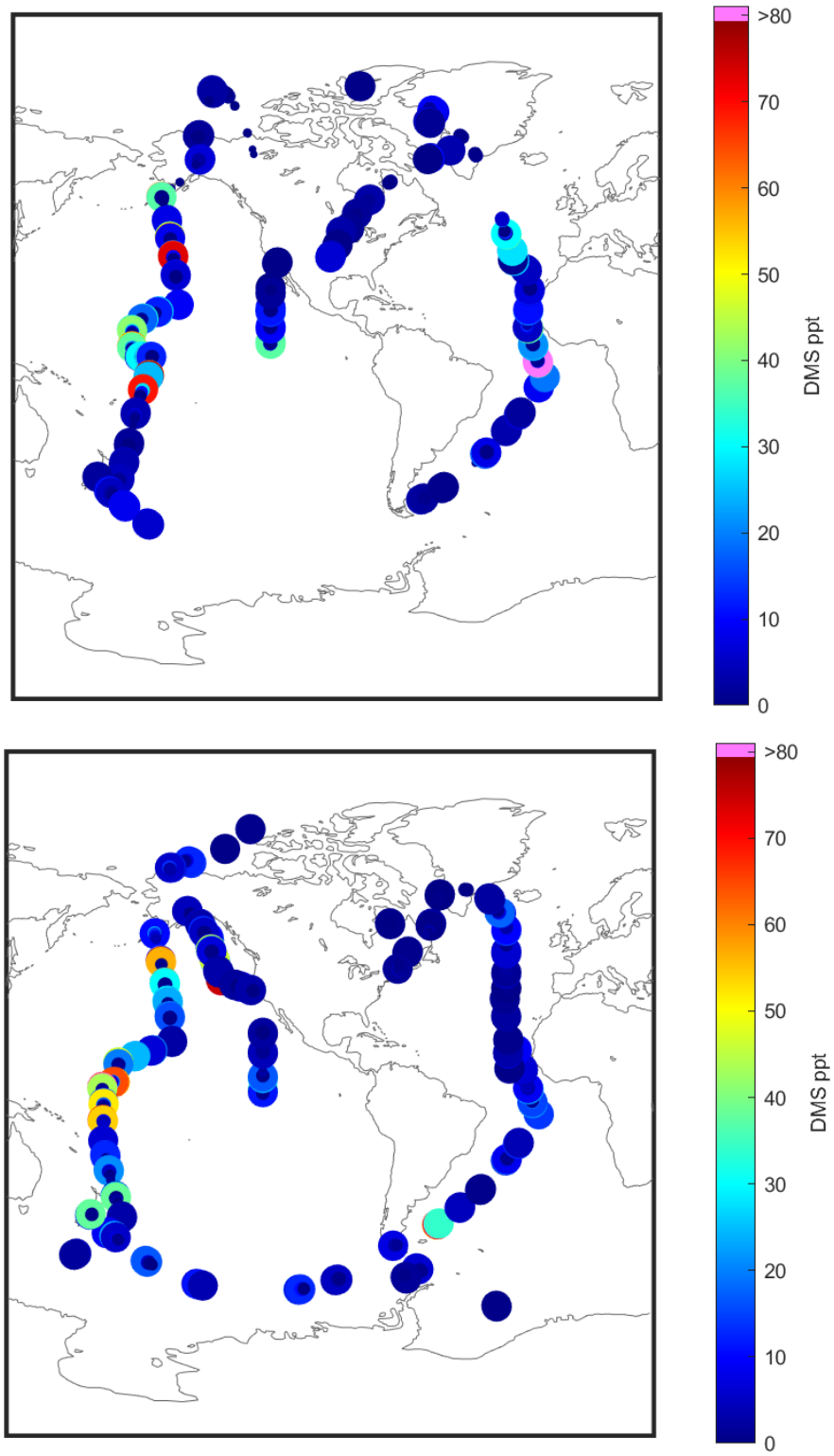

Figure 4.2 DMS during ATom 1 & 3. Larger markers indicate lower altitude. Altitude range from ~ 500 – 40000 ft.

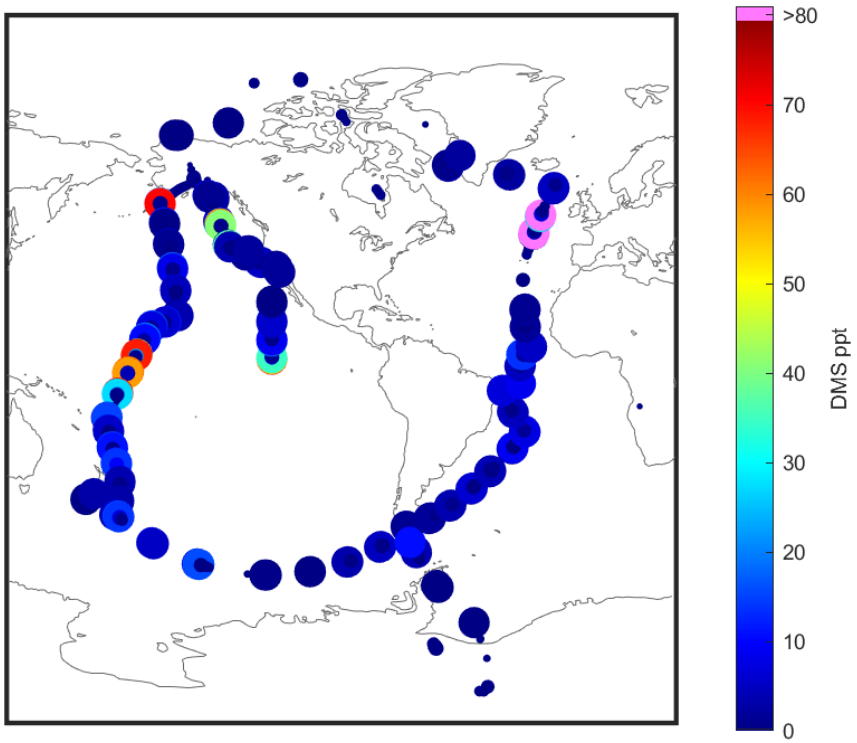

Figure 4.3 DMS during ATom 4. Larger markers indicate lower altitude. Altitude range from ~ 500 – 40000 ft.

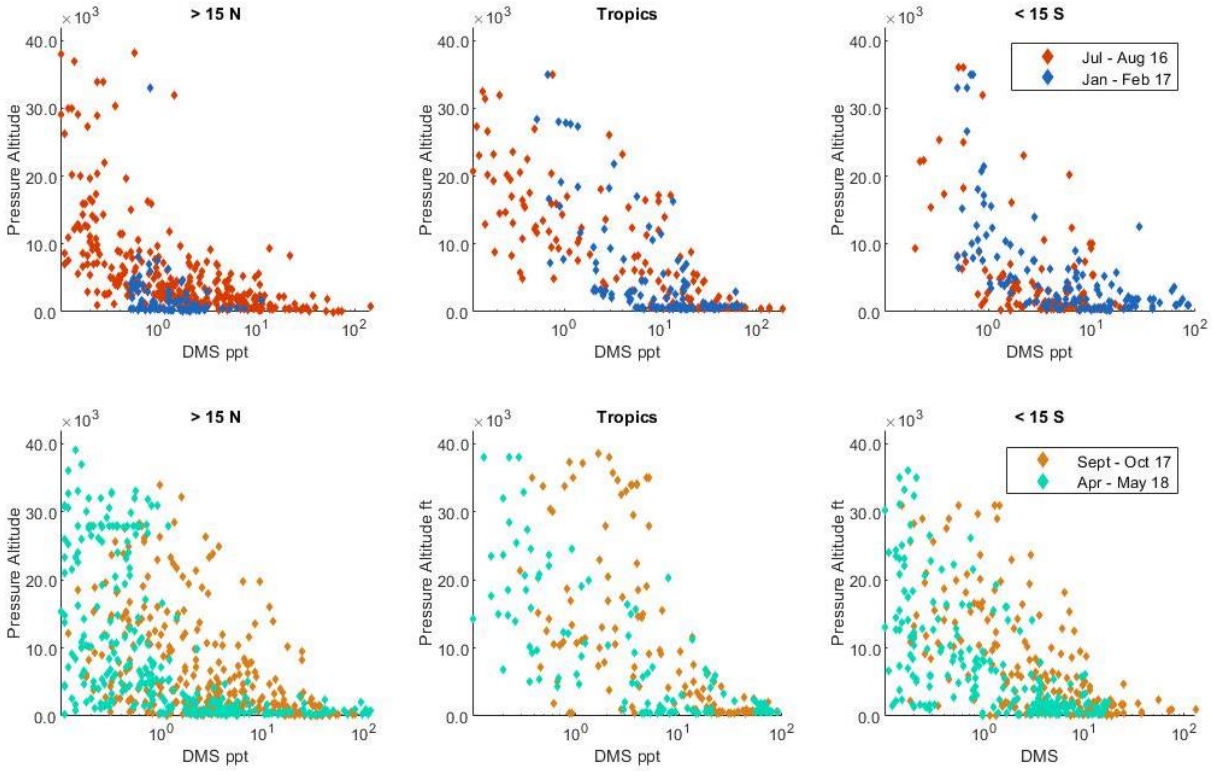

Figure 4.4 DMS vertical profiles during ATom 1-4.

4.2 Seasonal Trends in Global DMS

Mixing ratios of DMS tend to follow latitudinal seasonal trends on the global scale. However, looking at smaller scales introduces more variability. Some of the largest seasonal fluctuations were observed in the Southern Ocean, a region of enhanced marine productivity. In the Austral winter, most samples were below LOD, while in summer there were consistent low altitude observations of ~ 80 ppt DMS. Figure 4.5 shows latitudinal cross sections of DMS mixing ratios across seasons. Interestingly, much of the oceans do not seem to follow a summer/maximum, winter/minimum pattern. Currently, the spatial/temporal heterogeneities in DMS production cannot be reproduced with climatologies, annual averaging, or interpolation of *in situ* data that is available (Galí et al., 2018). And hence, models can only reproduce coarse features in DMS spatial/temporal trends (Bopp et al., 2003). Without more data, it is difficult to

discern if these measurements only encompass interseasonal effects, or if there are significant interannual fluctuations in effect as well.

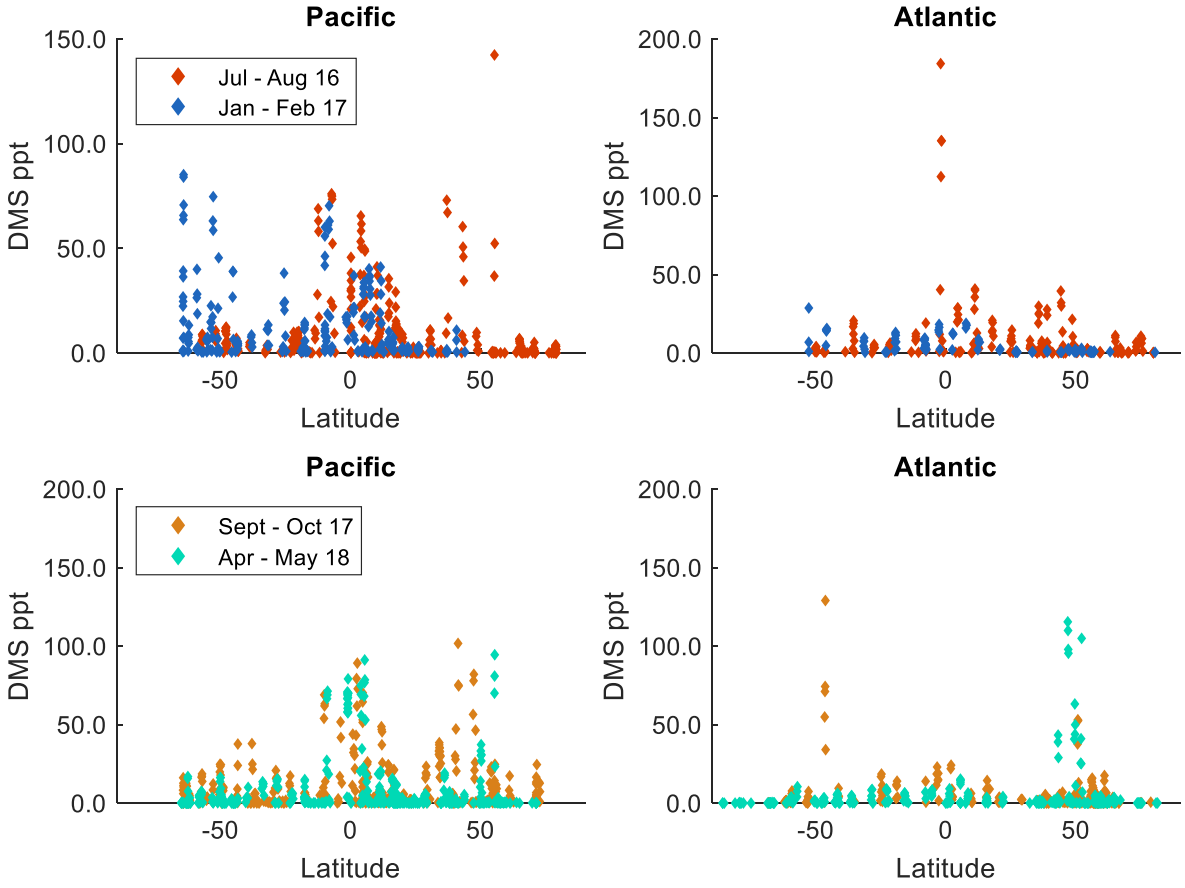

Figure 4.5 Seasonal comparison of DMS across the Pacific and Atlantic Oceans.

4.3 Potential Impacts on Aerosol and Cloud Condensation Nuclei

DMS emissions incorporate into aerosol primarily through oxidation to H_2SO_4, although there is evidence that methanesulfonic acid (MSA) may also be a contributor to aerosol loading (Hodshire et al., 2019). Once formed, these particles effect the local radiative balance through direct/indirect aerosol effects or growth into cloud condensation nuclei (CCN), which influence cloud formation and albedo (Andreae et al., 1995). The influence of DMS emissions on aerosol is heavily dependent on the concentration and characteristics of the aerosol. These conditions determine whether DMS will condense onto existing particles or favor new particle formation (Gali et al., 2019). The remote atmosphere is often pristine, with fewer aerosol for DMS

oxidation products to condense upon. This promotes the formation of ultrafine particles, that can grow large enough to act as cloud condensation nuclei (CCN). During the Atom deployments, a wide range of conditions demonstrated the heterogeneities of DMS influence on aerosol. The suite of aerosol instruments aboard the DC-8 allowed for the simultaneous measurement of particle composition and physical properties from ultrafine to coarse mode particles. For the ATom mission, the definition of accumulation mode particles was chosen to be a diameter of 0.6 to 0.5 μm, as it approximates the concentration of CCN at typical liquid water supersaturations (Brock et al., 2019). While in continental locations it is usual to use 1.0 or 2.5 μm as the upper limit for the accumulation mode, data from the NOAA particle analysis by laser mass spectrometry (PALMS) instrument showed that dust and seasalt particles dominated the number and mass concentrations for particles with $D_p \geq 0.50$ μm. For the ATom dataset, choosing 0.50 μm as the upper limit of the accumulation mode allowed for a more clear separation between secondary (nucleation, Aitken and accumulation modes) and primary particles (Brock et al., 2019). Figure 4.6 exhibits contrasting particle data for selected flights with elevated DMS mixing ratios during ATom 1 and 2. The CARE Cloudindicator data product (Figure 4.6) distinguishes between periods inside and outside of clouds, as well as the cloud phase, including aerosol cloud transition regime (Weinzierl, 2020). This data product is based on an algorithm that incorporates data from the cloud, aerosol and precipitation spectrometer (CAPS) as well as temperature and relative humidity data from the other instruments aboard the DC-8.

The first three panels of Figure 4.6 compare DMS emissions and particle data during a flight over the Southern Ocean (Figure 4.7) during the Austral summer, an area of elevated DMS emission. High DMS mixing ratios correspond to increased number concentration of accumulation mode particles (N_{acc}) as well as liquid/mixed phase cloud regions. Interestingly, the sulfate mass concentration for PM1 particles shows only minor correlation to DMS. In contrast, another flight beginning in the equatorial Atlantic (Figure 4.8) with elevated DMS

mixing ratios showed different features (Figure 4.6, second row). During this flight, DMS shows a clearer association with PM1 sulfate mass concentration than in the flight over the Southern Ocean. Figure 4.9 – 10 depict data for a flight over the northern hemisphere Atlantic during a season of increased biological activity (North Atlantic bloom). Unlike the previous flight data, these data show little association between DMS and various parameters related to particle composition and cloud formation, despite the DMS mixing ratios occasionally exceeding 100 ppt. While cloud formation is dependent on several factors, there were minimal cloud events despite the availability of CCN. But, while these flight transects were certainly different in many respects, measurements in these locations serve to highlight the variety of paths in which DMS can affect the aerosol-cloud interaction and influence radiative balance. The variability in the sources as well as the sinks of DMS, in the context of climate change, make understanding their impacts a moving target. As models and remote sensing techniques continue to develop, it will remain vital to continue *in situ* sampling on a global scale in order to contain the uncertainties introduced by DMS.

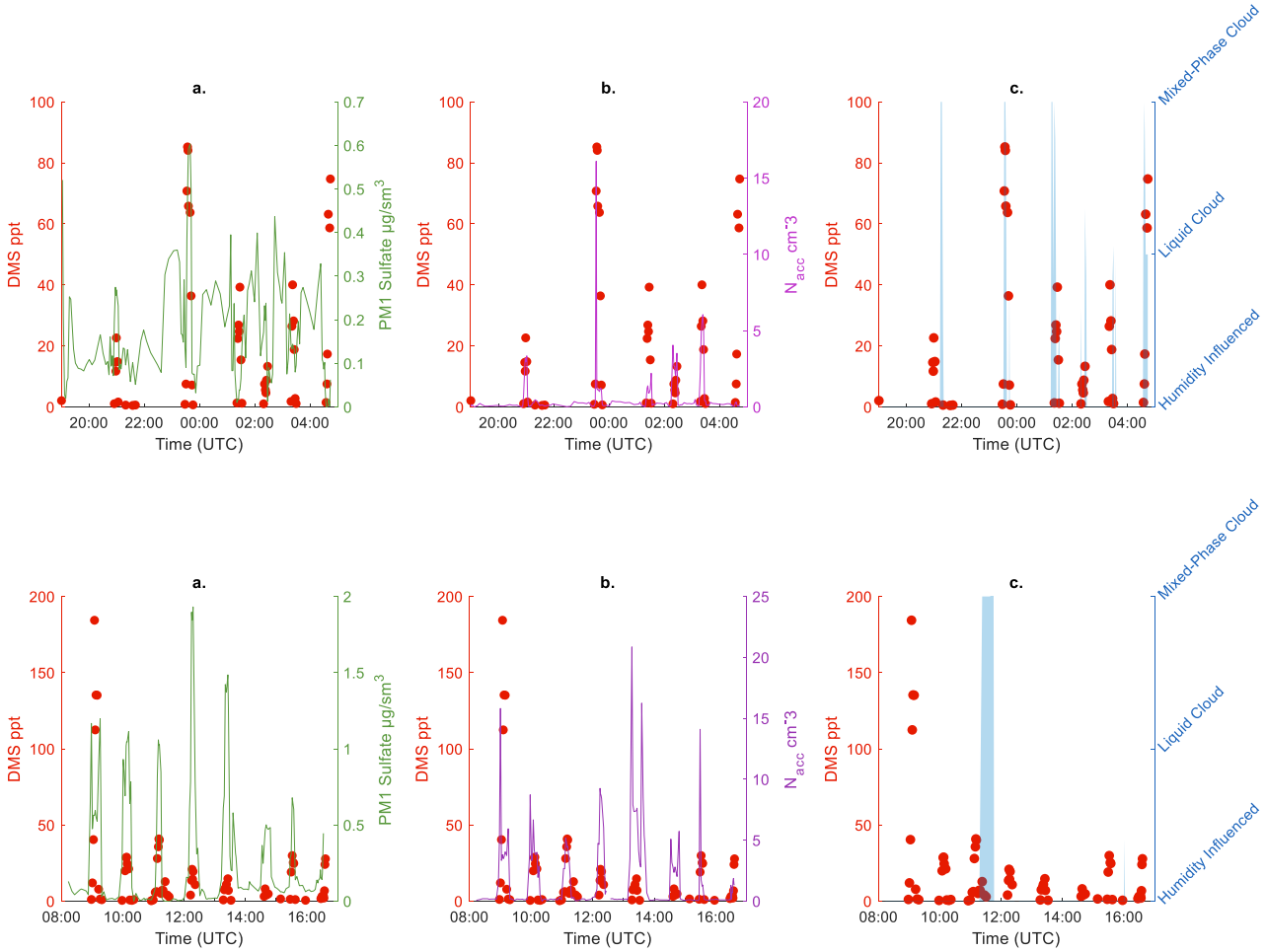

Figure 4.6 DMS mixing ratios and particle properties from a Southern Ocean flight (above, ATom 2) and from the tropical Atlantic (below, ATom 1). Sulfate mass concentration of PM1 data was provided by the CU Boulder HR-AMS. Number concentration of accumulation mode particles (0.6 to 0.5 µm) and Cloudindicator data product categorizes sample location into no cloud, humidity influenced aerosol, liquid cloud or mixed-phase cloud and is provided by the Vienna CARE instrument (Wofsy et al., 2018).

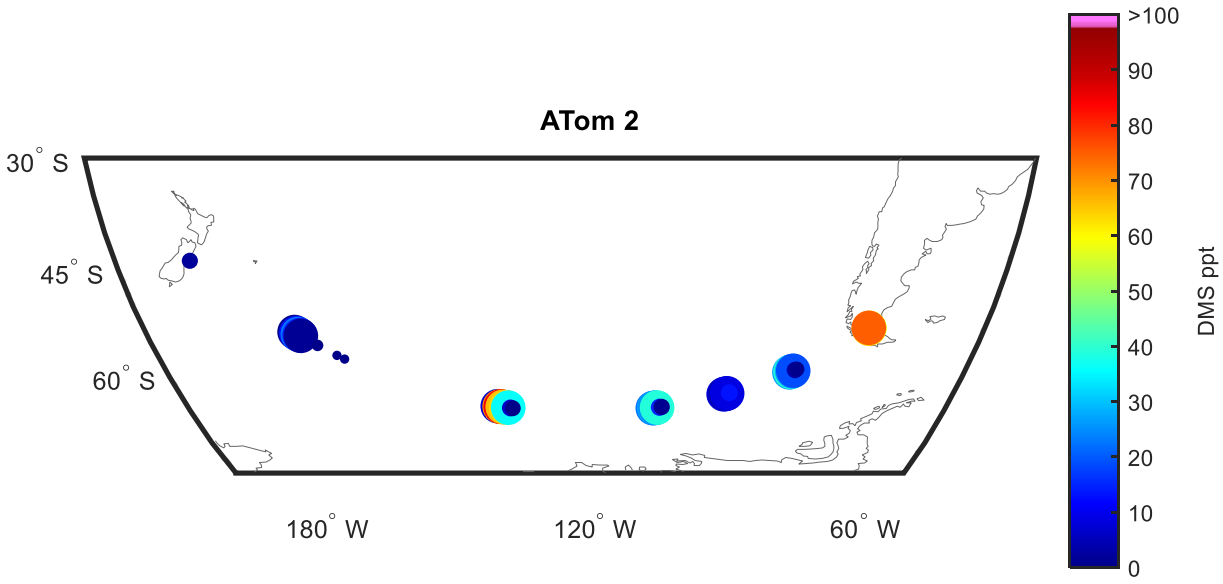

Figure 4.7 Flight path from ATom 2, flight 6. Larger markers denote lower altitude. Altitude range from ~ 500 – 40000 ft.

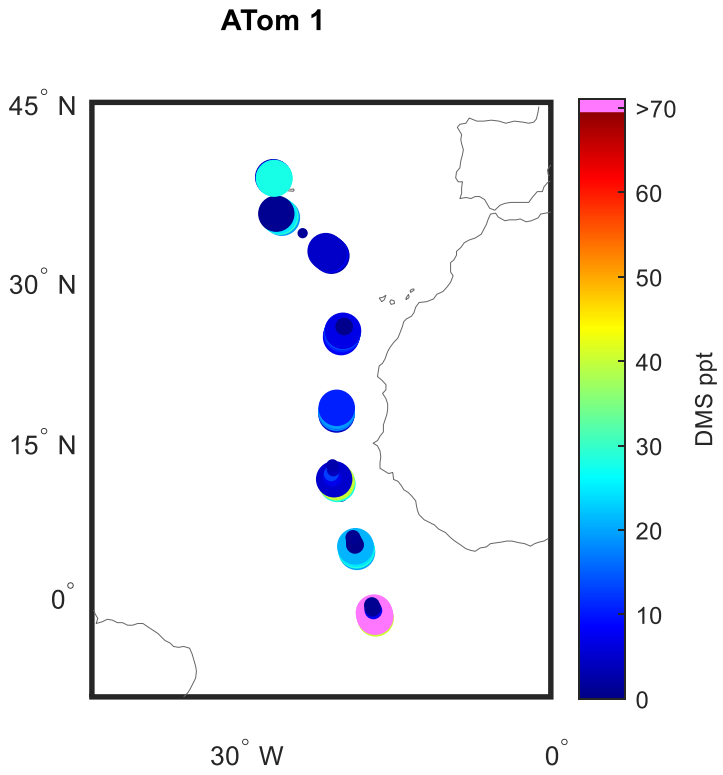

Figure 4.8 Flight path from ATom 2, flight 6. Larger markers denote lower altitude. Altitude range from ~ 500 – 40000 ft.

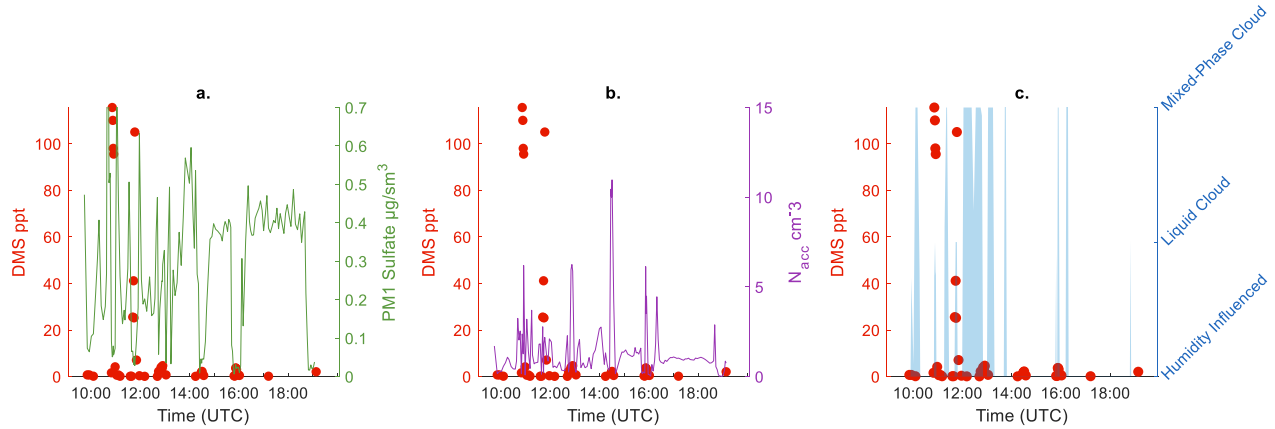

Figure 4.9 DMS mixing ratios and particle properties from a flight over the North Atlantic ATom 4). Sulfate mass concentration of PM1 data was provided by the CU Boulder HR-AMS. Number concentration of accumulation mode particles (0.6 to 0.5 µm) and Cloudindicator data product categorizes sample location into no cloud, humidity influenced aerosol, liquid cloud or mixed-phase cloud and is provided by the Vienna CARE instrument (Wofsy et al., 2018).

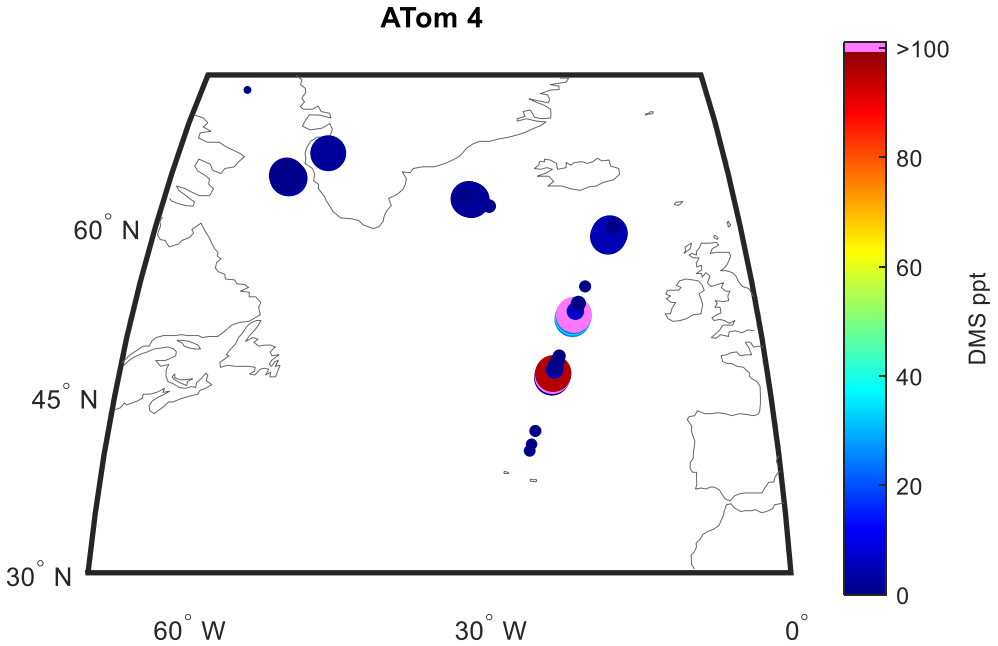

Figure 4.10 Flight path ATom 4, flight 10. Larger markers denote lower altitude. Altitude range from ~ 500 – 40000 ft.

4.4 The Role of DMS in a Changing Climate

As a major source of biogenic sulfur, it is imperative to understand the dynamics of DMS emission on interannual and decadal timescales. On the interannual timescale, ENSO events trigger localized changes to DMS emitters. As climate change impacts the frequency and severity of ENSO, understanding these changes will be key to predicting change in the earth system.

4.4.1 Effects of ENSO on DMS

On the interannual timescale, ENSO events trigger localized changes to DMS emitters. At the tropics, La Niña events result in increased ocean upwelling in the Eastern Pacific. These cooler, nutrient rich waters support plankton booms and the subsequent DMS-aerosol-cloud interaction result in a positive feedback, further cooling the region. The increases to atmospheric DMS mixing ratios are also attributed to the increased windspeed of these negative ENSO (La Niña) events. According to a recent modeling study, it is unclear whether windspeed or oceanic concentration of DMS has the larger effect on the increased shortwave cloud forcing (SWCF) observed during La Niña (Xu et al., 2016). The increased biological production may also have impacts on the vertical heat distribution of the ocean, as the larger plankton population performs photosynthesis, reducing the amount of light (heat) available deeper in the water column. El Niño, in comparison, suppresses tropical upwelling and surface windspeed, reducing the biological productivity as well as sea-to-air trace gas exchange.

In high latitudes such as the Arctic, where nutrient availability is not dependent on oceanic upwelling, ENSO events have contrasting effects. During El Niño, upwelling weakens, and the water column begins to become more stratified. This shallow, nutrient rich mixed-layer promotes a shift towards high DMS producing plankton groups (Wong et al., 2006). In contrast, La Niña deepens the oceanic mixed layer in arctic/sub-arctic regions, decreasing DMS emission by favoring different plankton species.

4.4.2 Effects of Climate Change on DMS Production

Projections of climate change effects on global net DMS production do not agree, with some projecting decreasing global levels (Six et al., 2013), and others increasing (Bopp et al., 2003). The complexity of various factors influencing DMS is considerable, involving physical aspects such as warming/weather as well as biological impacts like deoxygenation and ocean acidification (Hopkins et al., 2020). This complexity contributes to large spatial heterogeneities regarding projected DMS levels (Bopp et al., 2003). Decreases in polar ice cover, as well as warmer waters increase DMS production in certain areas (Gali et al., 2019). However, other impacts of climate change, such as ocean acidification or increasing severity of ENSO events, also affect DMS production. Ocean acidification has adverse effects on plankton and coral communities, two of the greatest marine DMS producers (Jackson et al., 2020). In addition, as warming increases, El Niño events will decrease in frequency yet increase in intensity, leading to stronger interannual variability. According to a modeling study, it is possible that increases in DMS may increase the frequency of La Niña events in the tropical pacific (Xu et al., 2016).

Atom data spans 2 ENSO events, with ATom 1 being during El Niño and ATom 3-4 deploying during a La Niña event. However, due to the heterogeneity of marine DMS production, it is hard to find anything conclusive without comparative measurements of DMS during ENSO events that correspond to the ENSO/season pairs observed during the ATom campaign. To further illuminate these impacts on atmospheric DMS, it is essential to continue with global sampling campaigns in the future that target interannual fluctuations (ENSO) as well as larger-scale perturbations (warming, anthropogenic influence).

REFERENCES

1. Veres, P. R.; Neuman, J. A.; Bertram, T. H.; Assaf, E.; Wolfe, G. M.; Williamson, C. J.; Weinzierl, B.; Tilmes, S.; Thompson, C. R.; Thames, A. B.; Schroder, J. C.; Saiz-Lopez, A.; Rollins, A. W.; Roberts, J. M.; Price, D.; Peischl, J.; Nault, B. A.; Moller, K. H.; Miller, D. O.; Meinardi, S.; Li, Q. Y.; Lamarque, J. F.; Kupc, A.; Kjaergaard, H. G.; Kinnison, D.; Jimenez, J. L.; Jernigan, C. M.; Hornbrook, R. S.; Hills, A.; Dollner, M.; Day, D. A.; Cuevas, C. A.; Campuzano-Jost, P.; Burkholder, J.; Bui, T. P.; Brune, W. H.; Brown, S. S.; Brock, C. A.; Bourgeois, I.; Blake, D. R.; Apel, E. C.; Ryerson, T. B., Global airborne sampling reveals a previously unobserved dimethyl sulfide oxidation mechanism in the marine atmosphere. *Proc. Natl. Acad. Sci. U. S. A.* **2020,** *117* (9), 4505-4510.

2. Gali, M.; Devred, E.; Babin, M.; Levasseur, M., Decadal increase in Arctic dimethylsulfide emission. *Proc. Natl. Acad. Sci. U. S. A.* **2019,** *116* (39), 19311-19317.

3. Sverdrup, H., On conditions for the vernal blooming of phytoplankton. *J. Cons. Int. Explor. Mer* **1953,** *18* (3), 287-295.

4. Andreae, M. O.; Crutzen, P. J., Atmospheric aerosols: Biogeochemical sources and role in atmospheric chemistry. *Science* **1997,** *276* (5315), 1052-1058.

5. Gaston, C. J.; Furutani, H.; Guazzotti, S. A.; Coffee, K. R.; Bates, T. S.; Quinn, P. K.; Aluwihare, L. I.; Mitchell, B. G.; Prather, K. A., Unique ocean-derived particles serve as a proxy for changes in ocean chemistry. *J. Geophys. Res.-Atmos.* **2011,** *116*.

6. Meinardi, S.; Simpson, I. J.; Blake, N. J.; Blake, D. R.; Rowland, F. S., Dimethyl disulfide (DMDS) and dimethyl sulfide (DMS) emissions from biomass burning in Australia. *Geophys. Res. Lett.* **2003,** *30* (9).

7. Galí, M.; Levasseur, M.; Devred, E.; Simó, R.; Babin, M., Sea-surface dimethylsulfide (DMS) concentration from satellite data at global and regional scales. *Biogeosciences* **2018,** *15* (11), 3497-3519.

8. Bopp, L.; Aumont, O.; Belviso, S.; Monfray, P., Potential impact of climate change on marine dimethyl sulfide emissions. *Tellus Ser. B-Chem. Phys. Meteorol.* **2003,** *55* (1), 11-22.

9. Hodshire, A. L.; Campuzano-Jost, P.; Kodros, J. K.; Croft, B.; Nault, B. A.; Schroder, J. C.; Jimenez, J. L.; Pierce, J. R., The potential role of methanesulfonic acid (MSA) in aerosol formation and growth and the associated radiative forcings. *Atmos. Chem. Phys.* **2019,** *19* (5), 3137-3160.

10. Andreae, M. O.; Elbert, W.; Demora, S. J., BIOGENIC SULFUR EMISSIONS AND AEROSOLS OVER THE TROPICAL SOUTH-ATLANTIC .3. ATMOSPHERIC DIMETHYLSULFIDE, AEROSOLS AND CLOUD CONDENSATION NUCLEI. *J. Geophys. Res.-Atmos.* **1995,** *100* (D6), 11335-11356.

11. Brock, C. A.; Williamson, C.; Kupc, A.; Froyd, K. D.; Erdesz, F.; Wagner, N.; Richardson, M.; Schwarz, J. P.; Gao, R. S.; Katich, J. M.; Campuzano-Jost, P.; Nault, B. A.; Schroder, J. C.; Jimenez, J. L.; Weinzierl, B.; Dollner, M.; Bui, T.; Murphy, D. M., Aerosol size distributions during the Atmospheric Tomography Mission (ATom): methods, uncertainties, and data products. *Atmos. Meas. Tech.* **2019,** *12* (6), 3081-3099.

12. Weinzierl, B., Personal communication, 3/6/2020.

13. Wofsy, S. C.; Afshar, S.; Allen, H. M.; Apel, E.; Asher, E. C.; Barletta, B.; Bent, J.; Bian, H.; Biggs, B. C.; Blake, D. R.; Blake, N.; Bourgeois, I.; Brock, C. A.; Brune, W. H.; Budney, J. W.; Bui, T. P.; Butler, A.; Campuzano-Jost, P.; Chang, C. S.; Chin, M.; Commane, R.; Correa, G.; Crounse, J. D.; Cullis, P. D.; Daube, B. C.; Day, D. A.; Dean-Day, J. M.; Dibb, J. E.; Digangi, J. P.; Diskin, G. S.; Dollner, M.; Elkins, J. W.; Erdesz, F.; Fiore, A. M.; Flynn, C. M.; Froyd, K.; Gesler, D. W.; Hall, S. R.; Hanisco, T. F.; Hannun, R. A.; Hills, A. J.; Hintsa, E. J.; Hoffman, A.; Hornbrook, R. S.; Huey, L. G.; Hughes, S.; Jimenez, J. L.; Johnson, B. J.; Katich, J. M.; Keeling, R.; Kim, M. J.; Kupc, A.; Lait, L. R.; Lamarque, J. F.; Liu, J.; McKain, K.; McLaughlin, R. J.; Meinardi, S.; Miller, D. O.; Montzka, S. A.; Moore, F. L.; Morgan, E. J.; Murphy, D. M.; Murray, L. T.; Nault, B. A.; Neuman, J. A.; Newman, P. A.; Nicely, J. M.; Pan, X.; Paplawsky, W.; Peischl, J.; Prather, M. J.; Price, D. J.; Ray, E.; Reeves, J. M.; Richardson, M.; Rollins, A. W.; Rosenlof, K. H.; Ryerson, T. B.; Scheuer, E.; Schill, G. P.; Schroder, J. C.; Schwarz, J. P.; St.Clair, J. M.; Steenrod, S. D.; Stephens, B. B.; Strode, S. A.; Sweeney, C.; Tanner, D.; Teng, A. P.; Thames, A. B.; Thompson, C. R.; Ullmann, K.; Veres, P. R.; Vizenor, N.; Wagner, N. L.; Watt, A.; Weber, R.; Weinzierl, B.; Wennberg, P.; Williamson, C. J.; Wilson, J. C.; Wolfe, G. M.; Woods, C. T.; Zeng, L. H., ATom: Merged Atmospheric Chemistry, Trace Gases, and Aerosols. ORNL Distributed Active Archive Center: 2018.

14. Xu, L.; Cameron-Smith, P.; Russell, L. M.; Ghan, S. J.; Liu, Y.; Elliott, S.; Yang, Y.; Lou, S.; Lamjiri, M. A.; Manizza, M., DMS role in ENSO cycle in the tropics. *Journal of Geophysical Research: Atmospheres* **2016,** *121* (22), 13,537-13,558.

15. Wong, C.-S.; Wong, S.-K. E.; Peña, A.; Levasseur, M., Climatic effect on DMS producers in the NE sub-Arctic Pacific: ENSO on the upper ocean. *Tellus B: Chemical and Physical Meteorology* **2006,** *58* (4), 319-326.

16. Six, K. D.; Kloster, S.; Ilyina, T.; Archer, S. D.; Zhang, K.; Maier-Reimer, E., Global warming amplified by reduced sulphur fluxes as a result of ocean acidification. *Nat. Clim. Chang.* **2013,** *3* (11), 975-978.

17. Hopkins, F. E.; Suntharalingam, P.; Gehlen, M.; Andrews, O.; Archer, S. D.; Bopp, L.; Buitenhuis, E.; Dadou, I.; Duce, R.; Goris, N.; Jickells, T.; Johnson, M.; Keng, F.; Law, C. S.; Lee, K.; Liss, P. S.; Lizotte, M.; Malin, G.; Murrell, J. C.; Naik, H.; Rees, A. P.; Schwinger, J.; Williamson, P., The impacts of ocean acidification on marine trace gases and the implications for atmospheric chemistry and climate. *Proc. R. Soc. A-Math. Phys. Eng. Sci.* **2020,** *476* (2237), 35.

18. Jackson, R. L.; Gabric, A. J.; Cropp, R.; Woodhouse, M. T., Dimethylsulfide (DMS), marine biogenic aerosols and the ecophysiology of coral reefs. *Biogeosciences* **2020,** *17* (8), 2181-2204.

CHAPTER 5

Conclusions

The ATom campaign successfully conducted 48 total research flights over 4 seasons, surveying the remote atmosphere from 82 °N to 86 °S, from 0-12.5 km in altitude. ATom accomplished many of its intended goals, including constructing a dataset for investigating the dynamics that control short lived climate forcers (O_3) in the remote atmosphere, as well as establishing a catalog of global background levels for trace gases, particles, meteorological data and photophysical data. As a part of the ATom payload aboard the NASA DC-8, the UCI WAS group measured 56 trace gases, including hydrocarbons, halocarbons, oxygenates, alkyl nitrates and sulfur species. This historical dataset is an invaluable record of the remote troposphere through all seasons, providing a baseline for future work investigating the effects of climate change on atmospheric dynamics.

This work focuses on the oceanic gases that were investigated as part of the ATom campaign. Of these, alkyl nitrates were observed to be an important source of reactive nitrogen to the remote atmosphere, with the C_1-C_4 nitrates contributing up to 88% of NO_y mixing ratios in the marine boundary layer. In general, the oceanic alkyl nitrates showed enhancements in areas of known biological activity, e.g., areas of strong ocean upwelling. Methyl nitrate was the most abundant alkyl nitrate measured throughout the campaign, and the least uniform in spatial and temporal distribution. The largest seasonal changes in methyl and ethyl nitrate measurements were observed in the tropics during the northern hemisphere spring and winter. Like i-propyl nitrate, 2-butyl nitrate showed the largest observed mixing ratios in urban outflows. However, observations of 2-$BuONO_2$ in the southern hemisphere boundary layer suggest that C_4 nitrates are emitted from the ocean. This has been suggested in previous work, but not included in recent modeling studies of ocean alkyl nitrates. This is most likely due to the

small contribution to marine boundary layer NO_y due to these compounds. More work will need to be done to study the oceanic source of C_{4+} alkyl nitrates. In addition, $MeONO_2$ showed a consistent disparity in boundary layer mixing ratios between the Pacific and Atlantic Oceans. Mixing ratios of $MeONO_2$ in the equatorial Pacific were a factor of 4 – 9 times larger than similar latitudes in the Atlantic. This difference is likely due to fundamental differences in ocean circulation between the two oceans, chiefly the strength of upwelling in the tropics. Although, there may be differences in nutrient availability beyond those caused by differences in ocean circulation. In addition to spatial and temporal trends, potential troposphere to stratosphere transport of alkyl nitrates at the equator was examined. Using models developed for VSLS, it was estimated that ~0.22 - 5.3 ppt of $MeONO_2$ could enter the lowermost stratosphere at the TTL during northern hemisphere spring. However, this is a coarse estimation. More robust modeling, as well as in situ measurements are needed to explore the extent of oceanic alkyl nitrates impact on stratospheric NO_y/O_3.

Oceanic emissions of dimethyl sulfide were examined due to their role in CCN production in the remote marine troposphere. Like alkyl nitrates, DMS was also enhanced in areas of marine primary productivity, including the equator and the Southern Ocean. In general, ocean circulation appears to exert strong control on DMS production, as it does for ocean alkyl nitrates. However, due to the biological nature of DMS formation in seawater, DMS did not show the same consistency in latitudinal gradient as other oceanic emissions. The global distribution of DMS coincided with plankton blooms and were more localized than enhancements in oceanic alkyl nitrate species. The largest seasonal difference in average DMS in the MBL were in the tropics, with the highest mixing ratios being measured in the North Atlantic during seasonal bloom conditions. While satellite measurements would be ideal to measure spatially variable gas species such as DMS, in situ sampling remains indispensable as more robust satellite instruments and algorithms are developed. More work needs to be done to

quantify the local radiative effects of the DMS aerosol-cloud relationship as DMS production distribution fluctuates temporally.

The measurements from ATom took place over the course of two years. During this time, there were two distinct ENSO events. While ATom provides excellent insight into the seasonal variability of oceanic species, it does not provide the temporal range necessary to examine the effects of interannual fluctuations (ENSO) or of perturbations with respect to climate change. In this respect, more in situ data collection is imperative to further our understanding of this chemistry in the context of climate change. This is especially important as ENSO has profound effects on ocean circulation, which strongly influences the production of oceanic species like alkyl nitrates and DMS. In the short term, ATom provides data fundamental to shaping environmental policy and mitigation strategies with respect to short lived climate forcers. In the long term, data from the ATom mission will allow for unprecedented studies in atmospheric chemical dynamics for decades to come, while also proving vital for the validation of next-generation satellites and chemical transport models.